# Neutron and X-ray Scattering Studies of Model Membranes

By

Erik Watkins
B.S. (Hampshire College, Amherst MA) 2001

DISSERTATION

Submitted in partial satisfaction of the requirements for the degree of
DOCTOR OF PHILOSOPHY
in
BIOPHYSICS
in the
OFFICE OF GRADUATE STUDIES
of the
UNIVERSITY OF CALIFORNIA
DAVIS

Approved:

Tonya L. Kuhl, Chair

Daniel L. Cox

Atul N. Parikh

Committee in Charge
2011





ProQuest LLC.
789 East Eisenhower Parkway
P.O. Box 1346
Ann Arbor, MI 48106 - 1346

Erik Benjamin Watkins
March 2011
Biophysics

# Neutron and X-ray Scattering Studies of Model Membranes

## *Abstract:*

Biological membranes, composed of a wide variety of lipid and protein molecules, are self-organized structures that define boundaries and compartmentalize space in living matter. Due to the complexity of true biological systems, fundamental physical studies often rely on simpler model systems. Here, neutron reflectometry (NR), x-ray reflectometry (XR), and grazing incidence x-ray diffraction (GID) were employed to investigate model bio-membranes. Using reflectometry, density profiles of supported membranes can be obtained as a function of depth with near atomic resolution. If the system diffracts, GID provides a sensitive probe of the local structure and packing of lipid molecules within the membrane. These techniques were implemented, and in the cases of XR and GID developed, to investigate the structure of single lipid bilayers on solid supports, bilayers on polymeric cushions, and protein binding interactions. For example, NR and XR studies revealed that bilayers containing PEG lipopolymers do not yield a hydrated cushion beneath the bilayer unless the lipopolymer can covalently bind to the underlying support. GID was used to

establish that dipalmitoyl-phosphatidylcholine (DPPC) lipids exhibit an orientational texture of their tilt directors and are always coupled across a single bilayer. Similarly, cholera toxin binding perturbed packing within model membranes resulting in the emergence of a textured lipid phase. In bilayers this altered order was transmitted to the opposing leaflet, representing a potential signaling mechanism. It is further hypothesized that textured micro-domains may intitiate clathrin independent endocytosis.

# CHAPTER I

# Investigating Model Bio-membranes Using Reflectometry and Grazing Incidence Diffraction

E. B. Watkins

Biophysics Graduate Group, University of California, Davis, 95616, USA

## *Abstract:*

This chapter provides background information on the relevance of model biological membrane systems and the use of neutron and x-ray surface sensitive scattering techniques to study them. A brief discussion of the theoretical background of reflectometry and grazing incidence diffraction (GID) measurements is included. Additionally, novel aspects of the data analysis methods used throughout this dissertation is described. Advantages of applying iterative model independent fitting of x-ray reflectivity data to yield scattering length density ribbons are shown. For grazing incidence diffraction analyses, approximations of the lipid tail as a cylinder and as series of scattering centers on a line are compared. The application of GID and Monte Carlo simulation to the study of orientationally textured lipid arrangements is also discussed.

## *Introduction:*

Cells are highly organized structures with many functional units or organelles defined by one or more membranes. These biological membranes are extremely complex and highly organized thin films consisting of a myriad of lipids and proteins. A broad range of biological functions occur at these interfaces including protein binding to membrane receptors, protein mediated transport across the membrane, and biological signaling [1,2]. Frequently in the field of biophysics, the sheer complexity of biological systems renders them impenetrable to fundamental physical studies. As a result, an emphasis has been placed on simpler model systems where a particular feature or phenomena is separated and studied in a more controllable manner.

Lipids and their self-organizing structures have been broadly researched as models of cellular membranes. Model biological membranes are simplified versions of cellular membranes and are designed to mimic specific cellular functions. Advantages of model membranes include system simplification as well as the ability to construct smooth, lamellar membrane structures. The planar geometry enables the application of several surface sensitive techniques such as ellipsometry, surface plasmon resonance (SPR) spectroscopy, and neutron and x-ray scattering [3]. Surface sensitive neutron and x-ray scattering techniques provide powerful tools for acquiring structural information at near atomic resolution: reflectivity provides out-of-plane structural information while grazing incidence diffraction (GID) provides a sensitive probe of the local, molecular structure and packing of lipid molecules within single membranes [4,5].

## *Neutron and X-ray reflectivity:*

Reflectivity, R, is defined as the ratio of the intensity of neutrons or x-rays elastically and specularly scattered from a surface relative to that of the incident beam (Fig 1). When measured as a function of wave-vector transfer ($q_Z=|\boldsymbol{k}_{out}-\boldsymbol{k}_{in}|$ = $4\pi\sin\theta/\lambda$, where $\theta$ is the angle of incidence and $\lambda$ is the wavelength of the beam), the reflectivity curve contains information regarding the sample-normal profile of the in-plane average of the scattering length densities (SLD) [4]. Analysis is performed by fitting the reflectivity profile of a real-space model to the measured reflectivity curve yielding the average density structure normal to the interface. If one knows the chemical constituents of the investigated system and the SLD distribution, the concentration of a given atomic species at a particular depth can then be calculated.

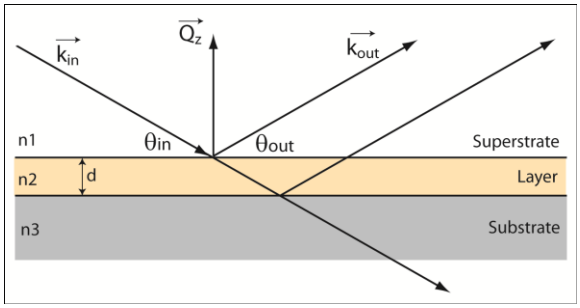


**Figure 1.** Schematic of reflectivity geometry. An incident beam (neutrons or x-rays) impinges on a planar sample at a glancing angle ($\theta_{in}$) and specularly reflects from the surface at the same angle ($\theta_{out}$). The momentum transfer vector, $q_z$, is the difference between the incoming wave vector ($k_{in}$) and the outgoing wave vector ($k_{out}$). Reflections from various interfaces in the sample interfere and the reflected intensity is measured as a function of $q_z$

The intensity of the specular reflectivity and the real space SLD are related by an inverse transformation. Since phase information is lost when collecting reflectivity data, a unique solution of the real space SLD profile cannot be

obtained analytically. To overcome this difficulty, various modeling methods are implemented which take an SLD profile, calculate the corresponding reflectivity curve, and iterate this procedure until a reasonable match between the calculated and measured reflectivity curves is obtained. One commonly used technique is the application of box models which parameterize layers within the sample according to their thickness, SLD, and interfacial roughness between layers. The reflectivity signal resulting from the real space profiles generated *via* this method are then calculated using the Parratt formalism [6]. This is a model-dependent method requiring *a priori* knowledge of the composition of the sample.

Model-independent methods, which do not require assumptions about the real space structure of the sample, can also be implemented to analyze reflectivity data. In one such method, the SLD profile of the data is composed of randomly generated smooth functions represented by cubic B-splines [7,8]. Starting from a random B-spline curve, a fitting procedure is applied to obtain B-spline curves that reproduce the measured reflectivity data. The fitting routine requires user inputted values for the difference in the SLD of the substrate and the subphase, $\Delta\rho$, number of B-splines to use, $n$, a dampening factor, $\beta$, and the distance between the substrate and the subphase, $d$. For computational optimization, the program used here further employs a function $A1$, which determines the smoothness of the solution with a weighting parameter $w1$, a biasing function $A2$, to bias the solution toward an expected average scattering-length density, and a second weight parameter $w2$, which weighs $A1/A2$ [7]. Curves with physical relevance to the system are chosen and refined by varying the parameters ($\beta$, $n$, $d$) to obtain fits that minimize the $x^2$ [7].

To further develop this method for reflectivity data analysis, thousands of iterations of the model-independent fitting procedure were run over a range of the input parameters [9]. A subset of the resulting SLD profile solutions were subsequently selected on the basis of physical relevance and $\chi^2$. Frequently, B-spline solutions that match the measured reflectivity exhibit highly oscillatory and unphysical SLD profiles. To eliminate these solutions, the derivative of each SLD profile was taken and the number of times the derivative changed sign was counted. Cases where this value was greater than a user determined cutoff were eliminated. Following the exclusion of highly oscillatory SLD profiles, solutions were selected on the basis of the $\chi^2$ of their fits. Typically, all solutions with a $\chi^2$ one greater than the minimum $\chi^2$ solution were accepted. The resulting set of profiles, usually 50-100, yielded a SLD ribbon representing the real space structure and the uncertainty of the structure (Fig. 2).

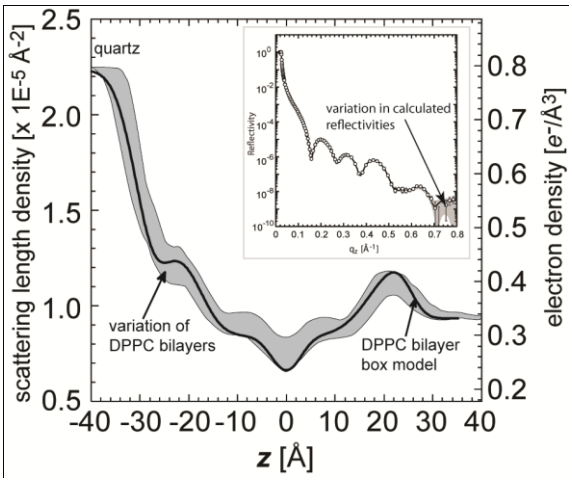


**Figure 2.** Electron density profiles for a DPPC bilayer obtained from a box model (black line) and model independent fitting (grey ribbon). The thickness of the ribbon represents uncertainty in the structure. The inset shows the XR data and a set of model independent fits (grey ribbon).

The model-independent method described provides substantial advantages over traditional box models because no *a prori* assumptions about the sample are required and it provides a measure of uncertainty of the obtained structure. However, one limitation of this technique is the requirement for data

with a sufficiently large $q_z$ range to result in a single set of valid solutions. Neutron reflectivity data, with typical maximum $q_z$ values around 0.2 – 0.3 $Å^{-1}$, is generally too small for the successful application of this model-independent method. In practice, this means that this technique is limited to higher resolution x-ray reflectivity measurements. Past x-ray refelectivity (XR) studies of lipid monolayers at the liquid-air interface have been very influential in the understanding of membrane structure [10]. However, until recently single biomembranes in bulk water had not been investigated due to experimental difficulties arising from attenuation and diffuse scattering of x-rays by water. High energy x-rays, in the 20 keV region, can be used to overcome these difficulties and study biological thin films at the solid-liquid (S-L) interface by XR with unprecedented resolution [11]. The increased resolution of XR over neutron reflectivity has allowed details of membrane biophysics to be addressed like membrane interactions with the solid support, and the influence of solution conditions and deposition technique on bilayer structure.

## *Grazing incidence x-ray diffraction:*

X-ray GID is a surface sensitive scattering technique that allows the characterization of thin crystalline or semi-crystalline layers at an interface and has the ability to provide in-plane structural information. Incident x-rays impinging on the sample at an angle less than the critical angle for total reflection generate an evanescent wave that propagates laterally along the interface (Fig 1). Since the amplitude of the evanescent wave decays exponentially with distance

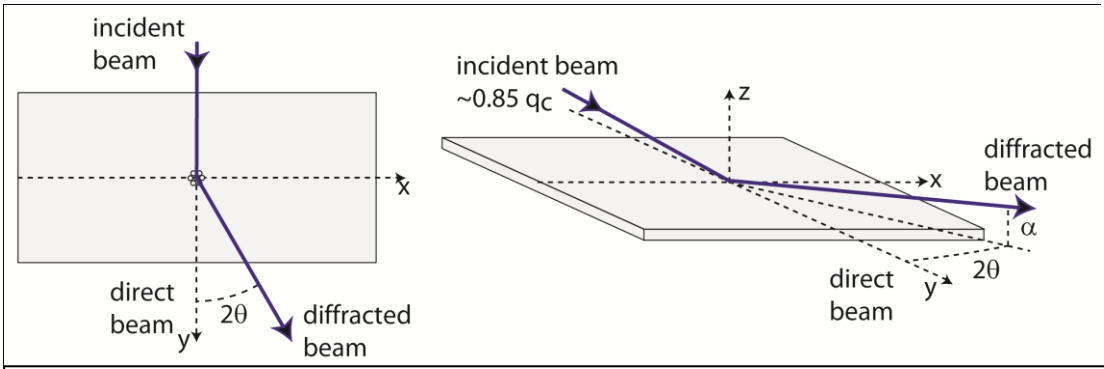


**Figure 3**. Schematic of grazing incidence diffraction geometry. An incident beam impinges on a planar sample below the angle for critical reflection. This generates an evanescent wave that travels along the interface and only penetrates the near surface region of the sample. The evanescent wave diffracts from in-plane ordered molecules at the surface and is measured as a function of $q_{xy}$ (corresponding the the $2\theta$ angle) and $q_z$ (corresponding to the $\alpha$ angle).

from the interface, this technique is well suited for studying surface layers [4]. The evanescent wave is diffracted by lateral two-dimensional order in a thin film (monolayer or bilayer). If the order is semi-crystalline, the evanescent wave Bragg scatters from domains that are oriented such that the angle $\theta_{hk}$ between the incoming radiation and the *(h,k)* lattice planes satisfy the Bragg condition, $\lambda = 2d_{hk}\sin\theta_{hk}$ (Fig. 4) [5]. In model membrane systems, grazing incidence diffraction from the packing of lipid tails can be used to provide information about the 2-D unit cell of the ordered domains and tilt orientations of the alkyl chains.

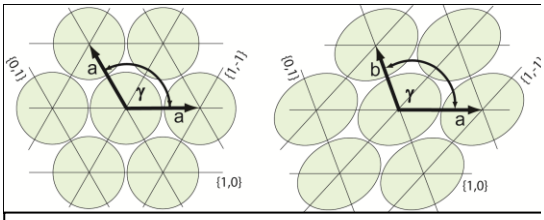


**Figure 4.** Schematic of 2-D unit cells. A hexagonal unit cell (left) is described using two equal unit cell vectors between molecular centers, *a*, that are 120° apart. An oblique or distorted hexagonal unit cell (right) is described using two unit cell vectors, *a* and *b*, and an angle between them $\gamma$ where $\gamma \neq 120°$. The scattering planes are labeled using the Miller indices {0,1}, {1,0}, and {1,-1}.

In GID experiments, scattered intensity is measured over a range of horizontal scattering vectors:

$$q_{xy} \equiv \left(q_x^2 + q_y^2\right)^{\frac{1}{2}}$$

$$= \frac{2\pi}{\lambda}\left[cos^2(\alpha_i) + cos^2(\alpha_f) - 2cos(\alpha_i)cos(\alpha_f)cos(2\theta_{xy})\right]^{\frac{1}{2}}$$

$$\cong \frac{2\pi}{\lambda}\left[1 + cos^2(\alpha_f) - 2cos(\alpha_f)cos(2\theta_{xy})\right]^{\frac{1}{2}}$$

where $2q_{xy}$ is the angle between the incident and diffracted beam projected onto the horizontal plane, $q_{xy}$ is the combination of horizontal components $q_x$ and $q_y$, and $\alpha_i$ and $\alpha_f$ are the incident and the scattered angles, respectively [5]. Bragg peaks are the intensity resolved in the $q_{xy}$–direction and integrated along the z-direction while the Bragg rod profiles are the intensity resolved in the $q_z$-direction and integrated over the $q_{xy}$ range of the Bragg peak. The positions of the maxima of the Bragg peaks allow the determination of the repeat distances $d = 2\pi/q_{xy}$ of the 2D lattice and from there the area per molecule. From the widths of the peaks it is possible to determine the average distance in the direction of the reciprocal lattice vector $q_{xy}$ over which there is near-perfect crystallinity.

While scattering from 3-D crystallites yields diffraction spots, scattering from 2-D systems does not require the Bragg conditions to be satisfied normal to the interface and results in Bragg rods. Bragg rods are the extension of Bragg peaks along $q_z$ and can be analyzed to provide information about the shape and orientation of the scattering objects in relation to the lattice planes. Diffraction from 2-D arrangements results in a continuous structure factor extending in the $q_z$ direction in reciprocal space. The structure factor intercepts the form factor of

the scattering objects and the product of the structure factor and the form factor yields Bragg rods.

For gel phase model lipid membranes, diffraction originates from the ordered packing of the lipid tails while head groups are typically are not well enough ordered to scatter coherently. Lipid tails are saturated hydrocarbons and their molecular shape can be approximated either as a cylinder or as a series of scattering centers, each representing a $CH_2$ group, arranged on a line (Fig. 5). To analyze the intensity distribution along a Bragg rod, the three main contributions to the diffraction signal must be considered: the structure factor, the form factor, and the interfacial roughness. While the structure factor determines the Bragg rod's position in $q_{xy}$, it only has an indirect influence on the intensity distribution along $q_z$ in the sense that the position in $q_{xy}$ will impact how the structure factor intercepts the molecular form factor. The form factor can be calculated by taking the Fourier transform of the real space molecular shape. In the case of cylindrical lipid tails, the form factor is an oblate ellipsoid in reciprocal space oriented perpendicular to the cylinder's long axis with the full width half maximum (FWHM) of the ellipsoid's thickness related to the cylinder's length by the equation FWHM=$2\pi/l$ (Fig. 6). The product of the structure factor

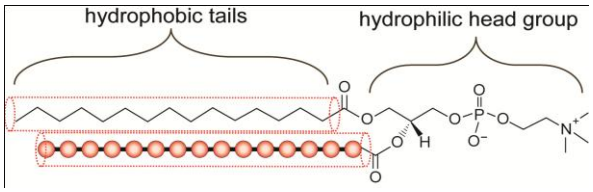


**Figure 5.** Molecular structure of a DPPC lipid. Diffraction from the lipid tails can be approximated using either the form factor of a cylinder (red outline) or as beads on a line where each bead represents a $CH_2$ group.

and molecular form factor depends on the orientation of the cylinders representing the lipid tails to the lattice planes. Each of the six lattice planes contributes to the Bragg scattering independently. If the 2-D lattice is hexagonal,

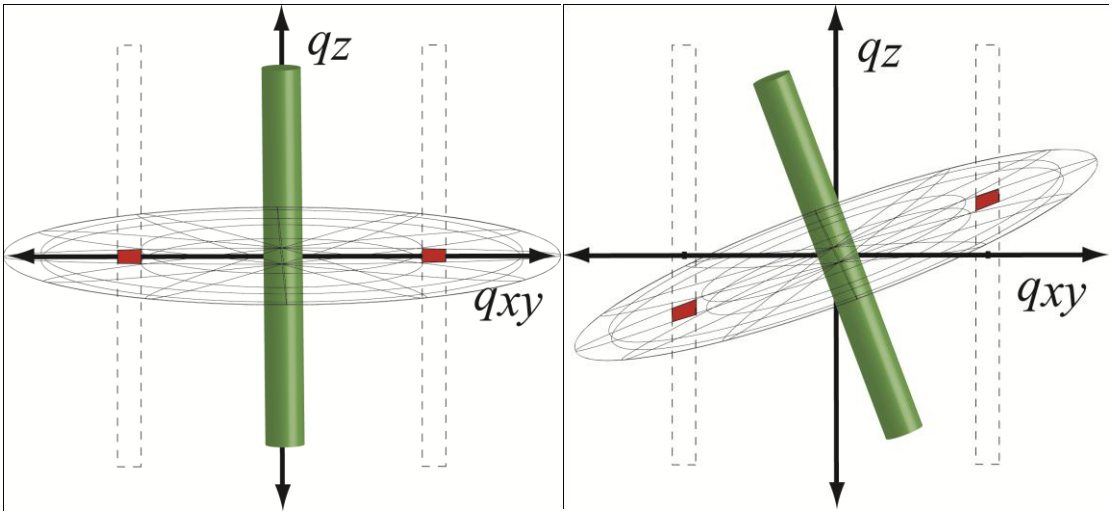


**Figure 6.** Schematic of cylindrical objects and their form factors. The form factor of a cylinder is an oblate ellipsoid normal to the cylinder's long axis. Dashed boxes indicate the location in $q$ of the structure factor for 2-D arrays of close packed cylinders. The red regions represent the intersection of the structure factor and form factor and correspond to the position in $q$ of the diffracted intensity. For an untilted cylinder (left), the diffracted intensity is center at $q_z$=0. The diffracted intensity is moved off the horizon when the cylinder is tilted (right).

all diffraction occurs at the same $q_{xy}$ position resulting in a single Bragg rod. However, if the molecules are tilted the hexagonal symmetry is broken and the single degenerate peak is split into up to three individual Bragg rods. Since each Bragg rod corresponds to an individual lattice plane, the orientation of a tilted cylinder in reference to the diffracting wave will be different for each reflection. For example, a cylinder may appear tilted from the perspective of one set of lattice planes and untilted from the perspective of another plane. As a result, the intersection of the form factor and structure factor will be at $q_z$=0 for lattice

planes that are orthogonal to the tilt direction and at higher $q_z$ for planes which are not (Fig. 6). After calculating the product of the form factor and structure factor, the Bragg rod intensity distribution is modulated by effects due to interfacial roughness and thermal fluctuations. This is taken into account using the Debye Waller (DW) factor which exponentially damps higher $q_z$ intensity as $e^{-q_z \cdot DW}$. Finally, the Bragg rod intensity distribution is altered by refraction from the interface described by the so called Vineyard-Yoneda peak [12]. Calculated Bragg rod profiles for diffraction from a lipid phase, shown in figure 7, demonstrate that approximating lipid tails as either cylinders or a series of scattering centers on a line are nearly equivalent.

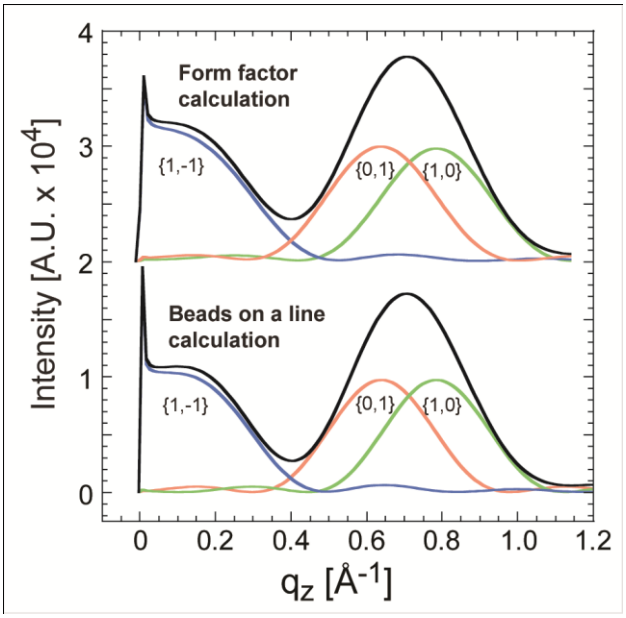


**Figure 7.** Bragg rod intensity distributions of diffraction from a 2-D arrangement of tilted cylinders representing a lipid gel phase. Calculations using the form factor of a cylinder (top) and using the Fourier transform of beads on a line (bottom) result in nearly identical intensity distributions.

Diffraction from ordered systems of long linear amphiphilic molecules like phospholipid tails is traditionally described as originating from arrangements of close packed molecules in 2-D hexagonal or distorted hexagonal unit cells. However, in certain systems diffraction from lipid tails exhibits a decreased intensity at or near $q_z$=0, indicating that all lattice planes are not contributing

equally to the overall diffraction, and cannot be described by any model involving the close packing of molecules. Instead, to model the diffraction requires a less dense packing arrangement of the molecules. This allows for a richer variety of lipid tail orientations including swirled phases consisting of azimuthal disorder of

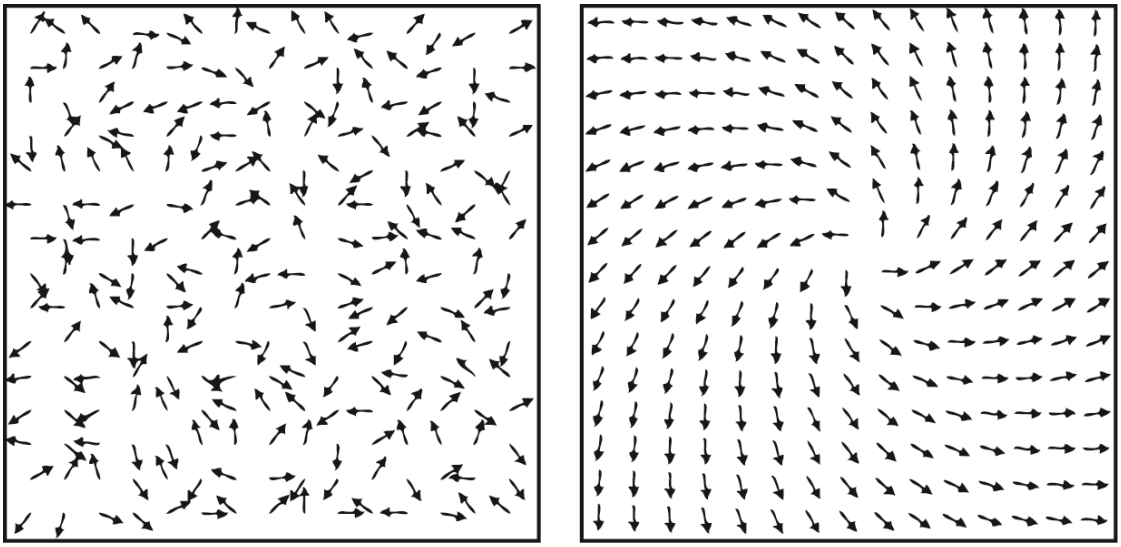

**Figure 8.** Director fields representing the tilt orientation of lipid tails. Tilt directors are vectors pointing along the lipids' alkyl chain backbones from the head group to the methyl end. The image on the left represents lipid molecules arranged on a hexagonal lattice with a random distribution of tilt orientations. The right image represents a textured lipid phase with a single center defect.

the tilt directors. Arrangements of lipid orientations can be described using a director field where tilt directions are represented by a set of vectors pointing along each lipid tail's alkyl chain. For example, figure 8 shows two director fields each consisting of lipids arranged on a 2-D hexagonal lattice with tail orientations equally distributed over all azimuthal angles. In one case (Fig. 8, left), the tilt orientations are randomly distributed while in the other case (Fig. 8, right) the director field consists of an orientational texture of lipid tilt directors centered around a single topological defect. Textures with a single centered defect or

disclination can be described using the equation $\phi = s \tan^{-1}(y/x) + \phi_0$ where $\phi$ is the azimuthal orientation of a molecule, $x$ and $y$ are the lateral coordinates of the molecule, $\phi_0$ impacts how the directors orient around the disclination, and $s$ is the strength of the disclination. For example, adjusting the angle parameter $\phi_0$ can result in a sink ($\phi_0 = \pi$), a source ($\phi_0 = 0$), or in concentric circles ($\phi_0 = \pi/2, \phi_0 = 3\pi/2$). Director fields with $s = \pm 1$ correspond to the lowest energy, symmetric textures and increasing values of $s$ generate higher energy configurations with more disordered textures and greater differences between the orientations of neighboring molecules. The director field shown on the right in figure 8 corresponds to an $s=1$, $\phi_0 = \pi/4$ texture. Although we can generate any arbitrary configuration of tilt directors, energetic considerations must be taken into account to determine if these arrangements are likely to exist in real systems. For example, large changes between the tilt directions of adjacent molecules would result in energetically unfavorable steric collisions. Additionally, even moderate changes in orientation between neighboring molecules reduce the van der Waals interactions thereby raising the systems free energy. By these arguments, the $s=1$ texture has a much lower energy state than a configuration consisting of randomly oriented tilt directors and system energy increases with increasing disclination strength.

For these types of systems the orientation of tilted lipids to the lattice planes is not the same for all molecules. Therefore, calculations using the form factor of a cylinder cannot be applied and, instead, the more flexible beads on a line approach must be implemented. This calculation is made by determining the

positions of all the relevant scattering centers in the system (CH2 groups in the case of lipid tails) and calculating the Fourier transform in the region of interest in reciprocal space. In a generalized notation, this calculation is of the form:

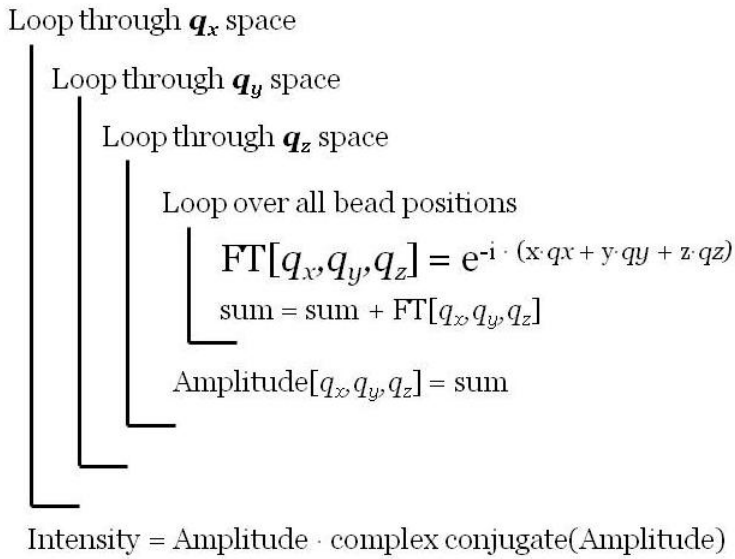


Figure 9 shows Bragg rods calculated using this method for the lipid arrangements in figure 8. Although both molecular arrangements consist of the same set of lipid orientations, the difference in their lateral placement and correlation between neighbors results in different diffraction patterns. In both cases, intensity at or near $q_z$=0 is lower than for the Bragg rod calculated for a similar close-packed lipid arrangement shown in figure 7. Further, the random arrangement of lipid orientations results in lower intensity near $q_z$=0 than the $s$=1 texture. This is consistent with the observed relationship between increasing strength of the texture and a decrease in low $q_z$ intensity.

The diffraction from any arbitrary arrangement of molecules can be calculated by the method described above. While random tilt orientations and textures with a single, centered defect can be useful models of the molecular

arrangements that give rise to a given diffraction signal, they may not be the best representation of the actual physical situation. To overcome this limitation, Monte Carlo simulation can be implemented to generate molecular arrangements within a lipid domain with a greater degree of physical significance. The first step is to identify constraints on the lipid order of the system. For example, protein binding to receptors in a membrane restricts the lateral position and in some cases the tilt orientation of the receptor molecules [13]. Assuming a lipid domain has a set of geometric constraints imposed on it, a Monte Carlo algorithm can be implemented to determine the minimum energy arrangement of the remaining lipids. A recipe to accomplish this task is outlined below:

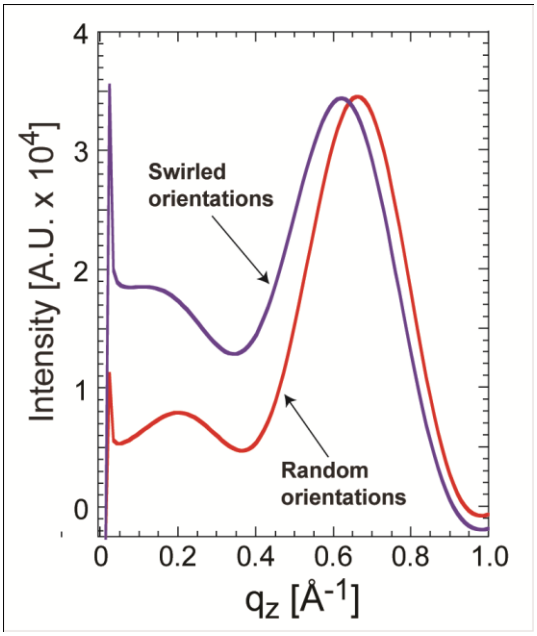


**Figure 9.** Bragg rod intensity distributions of diffraction from lipid domains with a random orientation (red) and an orientationally textured domain (blue) corresponding to the tilt director fields in Figure 9 are shown. The degree of texture impacts the intensity at low $q_z$.

1. Fix the position and orientation of constrained molecules.
2. Randomly pick a position for a new molecule adjacent to an existing molecule.
3. Assign a tilt direction to the selected molecule that minimizes the difference in orientation between it and neighboring molecules.
4. Repeat steps 2 and 3 until all available locations for molecules in the domain are filled.
5. Pick two molecules at random and calculate the average difference between each molecules tilt direction and the tilt directions of the neighboring molecules. A smaller average difference in tilt direction corresponds to a lower energy state.

6. If the system energy is lower when the orientation of the two randomly selected molecules are swapped, swap their orientations with a probability, p.
7. Repeat steps 5 and 6 until the system energy is minimized.

Using this method, molecular arrangements can be generated according to known physical attributes of the system and the associated scattering can be calculated and fit to the measured diffraction signal.

## *References:*


1. Krueger, S., *Neutron reflection from interfaces with biological and biomimetic materials [Review].* Current Opinion in Colloid & Interface Science, 2001. **6**(2): p. 111-117.
2. White, S.H. and W.C. Wimley, *Membrane protein folding and stability: Physical principles.* Annual Review of Biophysics and Biomolecular Structure, 1999. **28**: p. 319-365.
3. Sackmann, E., *Supported Membranes - Scientific and Practical Applications.* Science, 1996. **271**(5245): p. 43-48.
4. Kjaer, K. *Some simple ideas on X-ray reflection and grazing-incidence diffraction from thin surfactant films.* Physica B, 1994. **198**(1):p. 100-109
5. Alsnielsen, J., et al., *Principles and Applications of Grazing Incidence X-ray and Neutron Scattering from Ordered Molecular Monolayers at the Air-Water Interface [Review].* Physics Reports-Review Section of Physics Letters, 1994. **246**(5): p. 252-313.

6. Parratt, L.G., Surface *studies of solids by total reflection of x-rays*. Phyical Review, 1954, **95**(2): p. 359-369.

7. Pedersen, J. S.; Hamley, I. W. *Analysis of neutron and x-ray reflectivity data by constrained least-squares methods*. Physica B, 1994, **198** (1-3): p. 16-23.

8. Berk, N.; Majkrzak, *Using parametric B-splines to fit specular reflectivities*. Physical Review B, 1995, **51**(17): p. 11296-11309.

9. Watkins, E.B., et al., *Structure and Orientational Texture of Self-Organizing Lipid Bilayers*. Physical Review Letters, 2009. **102**(23):

10. Daillant, J.; Benattar, J.J.; Bosio, L. X-ray reflectivity study of monolayers of amphiphilics at the air-water interface. Journal of Physics-Condensed Matter, 1990, 2: p. SA405-SA410

11. Miller, C.E.; Majewski, J.; Gog, T; Kuhl, T.L. *Characterization of single biological membranes at the solid-liquid interface by x-ray reflectivity*. Physical Review Letters, 2005, **94**(23): 238104

12. Vineyard, G.H. Grazing-incidence diffraction and the distorted-wave approximation for the study of surfaces. Physical Review B, 1982, 26: p. 4146-4159.

13. Watkins, E.B.; Miller, C.E.; Majewski, J.; Kuhl, T.L. *Membrane Texture Induced by Specific Protein Binding and Receptor Clustering: Active roles for lipids in cellular function*. PNAS, under review.

# CHAPTER II

# Structure and Orientational Texture of Self-Organizing Lipid Bilayers

E. B. Watkins[*†], C. E. Miller[†], D. J. Mulder[‡],T. L. Kuhl[‡¶],J. Majewski[†]

[*] Biophysics Graduate Group, University of California, Davis, 95616, USA
[†]Manuel Lujan Neutron Scattering Center, Los Alamos National Laboratory, Los Alamos, NM, 87545, USA
[‡]Department of Chemical Engineering and Materials Science, University of California, Davis, 95616, USA
[¶] Department of Biomedical Engineering, University of California, Davis, 95616, USA

## *Abstract:*

The structure of single supported dipalmitoyl-phosphatidylcholine (DPPC) bilayers prepared by vesicle fusion or Langmuir-Blodgett/Schaeffer (LB/S) deposition techniques was characterized by x-ray reflectivity and grazing incidence diffraction in bulk water. LB/S bilayers display symmetric leaflets similar to monolayer structures, while vesicle fusion yields more inhomogeneous bilayers. Diffraction establishes that lipids are always coupled across the bilayer even when leaflets are deposited independently and suggests the existence of orientational texture.

## *Introduction:*

Lipids and their self-organizing structures have been broadly researched as models of cellular membranes and for their potential in biosensor applications [1]. In this work we report high resolution characterization of single, supported membranes composed of the most commonly studied phospholipid, DPPC, the "hydrogen atom" of lipids, and a major component of cellular memebranes [2]. Gel phase DPPC bilayers exhibit limited positional and orientational order and are analogous to 2-D smectic-C liquid crystals. Bilayers were prepared on a solid support by fusion of small, unilamellar vesicles or Langmuir-Blodgett/Schaeffer (LB/S) deposition. Our goals in these studies were to answer the following questions: (*i*) Which preparation method yields complete, well packed membranes and how reproducible are these preparation methods? (*ii*) Does the presence of the solid substrate influence the membrane structure? (*iii*) Are ordered domains present in the bilayer and, if so, how does diffraction in a single bilayer compare to that observed in monolayer or multilayer structures [3, 4]?

## *Experimental section:*

X-ray reflectivity (XR) and grazing incidence diffraction (GIXD) are particularly well suited for such studies [3-7]. While XR measurements are sensitive to the electron density distribution along the surface normal, GIXD yields precise in-plane packing properties and correlation lengths of the ordered (diffracting) domains [8, 9]. Monolayer measurements were carried out at the BW1 (undulator) beam line at HASYLAB (Hamburg), at a wavelength of

$\lambda$=1.304Å. Bilayer measurements were carried out at beamline 6-ID at the Advanced Photon Source (Argonne National Laboratory) at $\lambda$ = 0.545Å, which enabled measurements through a 1cm thick water layer.

The formation of a single DPPC bilayer at the quartz-water interface was verified by XR. Four different sample preparations and multiple regions on each sample were measured for both LB/S and vesicle fusion. For vesicle fusion, unilamellar vesicles ~500 Å in diameter were formed using a tip probe sonicator and incubated with UV ozone cleaned quartz substrates for 30 minutes prior to rinsing. For bilayers formed by LB/S, DPPC monolayers were deposited at 45mN/m using a Langmuir trough.

## *Results and Discussion:*

### *X-Ray Reflectivity*

**Fig. 1a** shows the measured reflectivity data of a representative LB/S DPPC bilayer (DPPC45) compared to a DPPC monolayer at 40mN/m. The data was analyzed using a model-free approach based on cubic B-splines [10] to obtain the electron density profile normal to the interface, $\rho(z)$. We performed over a thousand refinements within the parameter space and present a family of models for each reflectivity data set, all of which satisfy $\chi^2 \leq \chi^2_{min}+1$. The superposition of the profiles, after excluding non-physical oscillating profiles, yielded a broad electron density "ribbon" which is a measure of the uncertainty in the real space structure (**Fig. 1b)**. The more controlled LB/S deposition method (DPPC45 –

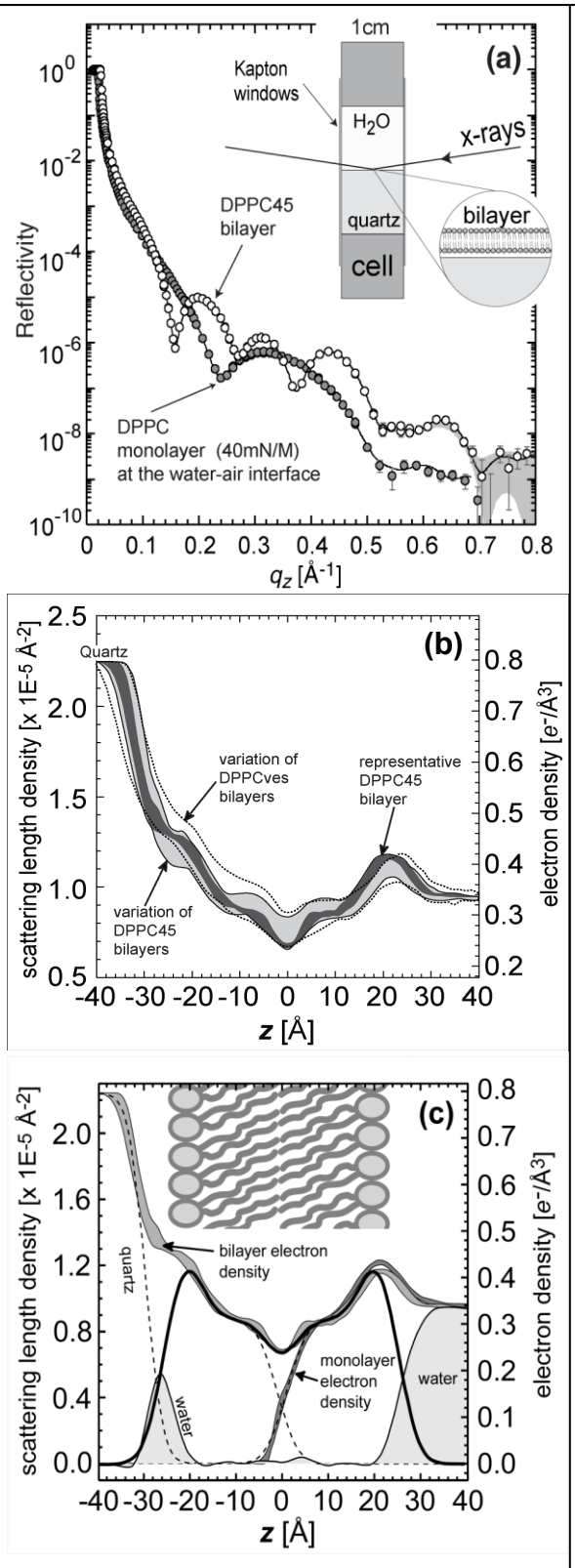


**Figure 1:**

**(a)** XR for a DPPC bilayer (DPPC45) deposited at 45mN/m at the quartz-$H_2O$ interface by LB/S and a DPPC monolayer at the air-water interface at a surface pressure of 40mN/m. Symbols represent measured data and solid lines are fits corresponding to $\rho(z)$ shown in (b) and (c). The thick gray curve shows the family of fits within the selection criteria with $\chi^2$ values between 2.0 and 3.0.

**(b)** Scattering length density profiles of DPPC bilayers. The gray curve demonstrates the LB/S (DPPC45) bilayer structural variation over approximately a dozen measurements and four sample preparations. The dotted curves encompass the variation of vesicle fusion bilayers (DPPCves) and show a perturbation to the inner leaflet structure. The width of the dark "ribbon" corresponds to profiles generated from reflectivity fits plotted in (a), and depicts a measure of uncertainty in the real space structure. 0 Å denotes the center of the bilayer.

**(c)** Volume constrained model for the representative DPPC45 bilayer profile (dark ribbon in b). The black line is the lipid contribution to the total electron density. The dark gray curve is the scattering length density profile of a DPPC monolayer at 40mN/m corresponding to the monolayer reflectivity in (a).

gray shaded area) yields a more symmetric structure compared to bilayers formed by vesicle fusion (DPPCves – dashed lines).

In **Fig. 1c** the $\rho\ (z)$ for a high coverage DPPC45 bilayer is shown in comparison with a DPPC monolayer at the air-water interface at a surface pressure of 40mN/m. To extract physical parameters from the model independent fitting, we constructed a volume constrained mean field model by defining four electron contributors: lipid headgroups (choline up to and including the two carbonyls), lipid tail regions, the quartz substrate, and water. A single leaflet was therefore a two step function: one for the higher electron density of the head group and the other for the lower electron density tails. The electron density of each region was constrained by the known volume of a DPPC headgroup (319Å$^3$) [11] and tail (785Å$^3$), and a value of 40.8Å$^2$ for the cross-sectional area of two hydrocarbon chains perpendicular to the molecular backbone [12]. Step function profiles were convolved with Gaussians to represent interfacial roughness. With these described volume constraints and the constituent atoms of a DPPC lipid, parameters corresponding to the molecular tilt, position of the each leaflet vis-à-vis the interface, and coverage of each leaflet were varied independently to represent the DPPC45 bilayer $\rho\ (z)$. The best model (**Fig. 1c**) gave a symmetric distribution of $\rho\ (z)$ across lipid leaflets, showing that the substrate does not induce significant changes to the inner leaflet. The bilayer out-of-plane RMS roughness of 3.8Å is only slightly greater than the 3Å RMS substrate and indicates that the bilayer is nearly conformal with the support. The extracted molecular tilt angle for the hydrocarbon tails was 27.3°, consistent with previous work for DPPC monolayers [13] and multilayers in the gel-phase [14],

and corresponds to an average area per lipid of 45.9Å$^2$. The distance between the quartz interface and the headgroup region of the inner leaflet was 4.2Å. This "water cushion" matches well with previously measured phosphatidylcholine single bilayers [15], and refutes the presence of a thicker water cushion under supported bilayers [1]. The lipid headgroup hydration was determined by assuming regions of electron density in the profile not accounted for by lipids or quartz to be attributable to water (gray areas in **Fig. 1c**). On average 4.5 water molecules are associated per headgroup in the outer leaflet compared to 6.5 water molecules per headgroup in the inner leaflet. These values compare favorably with the 3.7 waters of hydration per DPPC headgroup reported in multilayer studies [11]. The modest increase in water per lipid in the inner leaflet of supported membranes can be considered the water "cushion".

Bilayers formed by vesicle fusion have a similar structure to LB/S bilayers with some notable differences: there is asymmetry in the electron density distribution between two lipid leaflets and a higher than expected electron density in the inner leaflet. The total thickness of the bilayer is also ~5% greater than those formed by LB/S. Greater disorder in the inner leaflet, resulting in electron density contributions from inner leaflet head groups displaced towards the bilayer center, can account for these features. Since no substrate induced structural changes were observed for DPPC bilayers deposited *via* LB/S, the perturbations in the inner leaflet of DPPCves can be associated with the vesicle fusion process.

***Grazing Incidence X-Ray Diffraction***

The GIXD images (**Fig. 2a)** show the scattering intensity as a function of $q_{xy}$ and $q_z$ for DPPC monolayers at surface pressures of 30, 40, and 50mN/m compared with single DPPC bilayers formed by LB/S deposition and vesicle fusion. The images reveal two peaks indicative of a distorted hexagonal lattice. The relative intensity distribution between the two peaks for the monolayers at each pressure obeys the 2:1 multiplicity rule which is evident after integration of the peaks (**Fig. 2b**). For bilayers, more of the intensity is associated with the out-of-plane, {(0,1), (1,0)} peak. This is similar to DPPC multilayers [16], suggesting that the observed diffraction is not altered by the quartz substrate. Bilayers formed by vesicle fusion, show less intense signal due to reduced in-plane order.

Bragg peaks ($q_{xy}$ resolved intensity) for DPPC monolayers and supported bilayers are shown in **Fig. 2b** and the unit cell parameters are presented in **Table 1**. The area per molecule, equivalent to that obtained from reflecitivity, matches well with monolayer data [13] and previously reported gel-phase DPPC multilayer work [12, 17]. Bragg rod (BR, $q_z$ resolved intensity) analysis enabled determination of whether (*a*) the lipid leaflets of the bilayer scatter independently or as one coupled entity and (*b*) the relative orientation of the tails in the inner *vs*. the outer leaflet. We discuss the BR analysis for the case of the DPPC45 bilayers (**Fig. 2c**). From the FWHM=0.15 Å$^{-1}$ of the {(0,1),(1,0)} BR at $q^{max}_z$ ~ 0.67 Å$^{-1}$ (**Fig. 2b**), the corresponding real-space length of the scattering entity is ~42 Å (~$2\pi$/0.15 Å$^{-1}$). This indicates that, although the leaflets are deposited independently, lipids in opposing leaflets self-organize and invariably couple to scatter in registry. There is no signature of the FWHM associated with

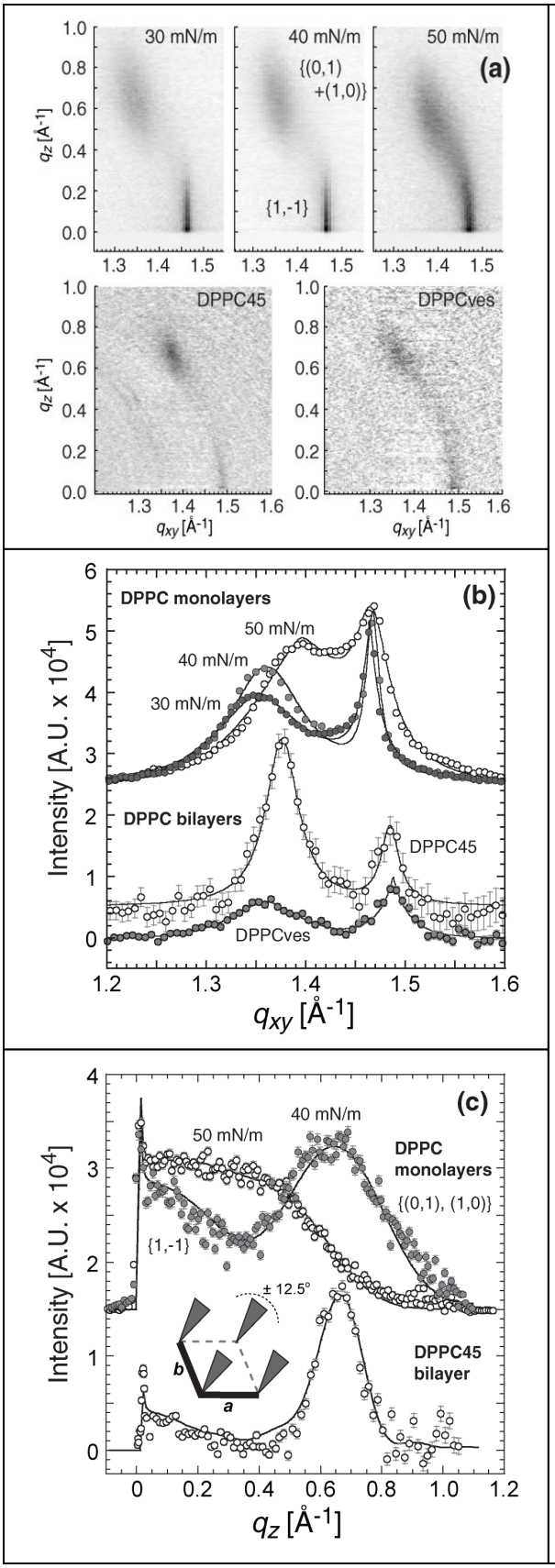


**Figure 2:**

**(a)** GIXD from DPPC monolayers at the air-water interface (top) and single bilayer membranes (bottom) at the quartz-water interface deposited by LB/S (DPPC45, left) and vesicle fusion (DPPCves, right). The projection of the water surface (monolayers) and quartz substrate (bilayers) is defined as $q_z$=0Å$^{-1}$. Two Bragg rods were observed. Miller indices, {(0,1)+(1,0)} and {1,-1}, corresponding to a distorted hexagonal unit cell are equivalent to the centered-rectangular unit cell notation used in multilayer structures where $\{1,1\}_{\text{rectangular}}$ corresponds to $\{(0,1), (1,0)\}_{\text{hexagonal}}$ and $\{0,2\}_{\text{rectangular}}$ corresponds to $\{1,-1\}_{\text{hexagonal}}$. For DPPCves, the curvature of the diffraction peaks along constant $q_{tot} = (q_z^2 + q_{xy}^2)^{1/2}$ is due to variablitiy in the tilt angle normal to the interface of the diffracting lipids.

**(b)** Bragg peaks from DPPC monolayers and bilayers. Solid lines are fits to the Bragg peaks using Voight functions.

**(c)** Bragg rods from DPPC monolayers and bilayers. Solid lines are fits to the models described in the text. The fit to the bilayer Bragg rod corresponds to the azimuthal disorder model (described in the illustration).

uncoupled lipids.

Contrary to typical monolayer diffraction [18], no arrangement of close packed cylinders was able to recreate the observed intensity distribution of the bilayer BRs. We therefore used a more flexible "beads on a line" approach to model non-close packed structures. The alkyl tails of the DPPC molecules were approximated as equidistant beads and the scattering intensity was calculated discretely for given molecular orientations within the bilayer. To describe the leaflets coupled as one scattering entity, thirty-two beads, each representing a $CH_2$, were arranged on a 42 Å line. We were successful in reproducing the measured scattering intensity of the BR with two different models. The first model introduced small random positional disordering orthogonal to the molecular tilt directors. As a result, the intensity of the {1,-1} BR was reduced. This model is satisfying due its simplicity and approximated the measured BR reasonably well (fit not shown). The second model created a 2D liquid crystal smectic phase with orientational texture through azimuthal perturbations to the molecular tilt directors and resulted in a better fit [19]. For our system, an end bead was fixed to the distorted hexagonal lattice obtained from Bragg peak fitting (**Table 1**) and the remaining molecule was tilted 26.8º from the surface normal. We created a normal distribution of azimuthal tilts with a HWHM of 12.5º centered at the nearest neighbor direction (**a**+**b**). To eliminate collision between molecules, only small differences in azimuthal tilt between adjacent chains was allowed (**Fig. 2c)**. This distribution of tilts is suggestive of bend domains observed in liquid crystals [20] but on a molecular scale. Other models including a lateral offset between leaflets [12] and a "kinked" orientation, where the

molecules in each leaflet had a different tilt direction relative to each other, were unable to fit the diffraction data.

Although the diffracted intensity was much weaker for DPPCves and the BR had greater on horizon intensity, neither the positional disordering or orientational texture model was able to fit the data unless variation in the normal tilt angle of the lipids was introduced. These variations in normal tilt and the weaker diffraction intensity are consistent with the greater disorder observed in the inner leaflet by reflectivity measurements.

## *Table 1:*

| **DPPC** | $\pi$ (mN/m) | In-plane *Bragg Peaks* | | | | Out-of-Plane *Bragg Rods* | | | |
|---|---|---|---|---|---|---|---|---|---|
| | | a, b (Å) | $\gamma$ (°) $\pm$ 0.2 | Area per molecule (Å$^2$) | Coherence Length $L_{xy}$ (Å) ±10.0 | Coherence Length, $L_c$ (Å) (cylinder height) | Tilt angle $t$ (°) | Tilt dir. (°) (from NN) | Red. $\chi^2$ |
| Mono-layers | 30 | 5.104 $\pm$ 0.002 | 114.4 | 47.43 ± 0.01 | $L_{10,01}$= 60 $L_{1-1}$= 350 | 19 | 31.0 | 10 | 15.1 |
| | 40 | 5.085 $\pm$ 0.002 | 114.7 | 46.97 ± 0.01 | $L_{10,01}$= 60 $L_{1-1}$= 415 | 19 | 30.6 | 10 | 19.3 |
| | 50 | 5.036 $\pm$ 0.002 | 116.0 | 45.36 ± 0.01 | $L_{10,01}$= 50 $L_{1-1}$= 140 | 19 | 25.8 | 14 | 13.6 |
| Bi-Layers | LB/S @ 45mN/m | 5.026 $\pm$ 0.01 | 114.7 | 45.9 ± 0.5 | * * | 42 | 26.8 | ±12.5 | 39.0 |
| | Vesicle Fusion | 5.046 $\pm$ 0.01 | 113.6 | 46.7 ± 0.5 | * * | | | | |

* Resolution limited. The limited $\Delta q_{xy}$ = 0.0267 Å$^{-1}$ resolution did not allow us to measure coherence lengths beyond 210 Å.

## *Conclusions:*

Together, XR and GIXD techniques provide means to measure the structure of self organizing molecularly thick films in bulk water with

unprecedented resolution. Our findings demonstrate that supported DPPC bilayers formed by vesicle fusion have more disorder in the inner leaflet compared to structures prepared using the more controlled LB/S technique. In both cases, only a modest water cushion was detected between the bilayer and support. Despite potential interactions with the substrate, the in-plane and out-of-plane structure of a single bilayer was found to be very similar to multi-lamellas. Diffraction clearly establishes that the leaflets are coupled, and that the bilayer self-organizes so that opposing lipid tails always scatter as one entity. A small variation in the azimuthal tilt direction of the lipid tails was able to fully reproduce the diffraction data in the case of LB/S. This variation in azimuthal tilt indicates an orientational texture of lipid molecules which may be an example of a molecular scale precursor to larger scale textures observed in many 2-D liquid crystalline systems [20]

## *References:*

[1] Sackmann, E. *Supported membranes: Scientific and practical applications*. Science, 1994. **271**(43): p. 43-48

[2] Kucerka, N., Tristram-Nagle, S. and Nagle, J.F. *Closer look at fully hydrated fluid phase DPPC bilayers*. Biophysical Journal, 2006. **90**(11): p. L83-L86

[3] Munster*, C., et al. Magainin 2 in phospholipid bilayers: peptiide orientation and lipid chain ordering studied by x-ray diffraction*. Biochimica et biophysica acta-Biomembranes, 2006. **1562** (37): p. 37-44

[4] Spaar, A., Munster, C. and Salditt, T. *Conformation of peptides in lipid membranes studied by x-ray grazing incidence scattering*. Biophysical Journal, 2004. **87**, (1):p. 396-407

[5] Daillant, J. *et al.*, *Structure and fluctuations of single floating lipid bilayer*. Proceedings of the National Academy of Sciences, 2005. **102**(33): p. 11639-11644

[6] Miller, C.E. *et al. Probing the local order of single phospholipid membranes using grazing incidence x-ray diffraction*. Physical Review Letters, 2008. **100**(5): 058103

[7] C. Reich *et al.*, *Supported membranes on polyelectrolyte layers studied by x-ray reflectometry*. Physica Status Solidi A, 2006. **203**(14): p. 3463-3467

[8] K. Kjaer *et al.*, *An x-ray scattering study of lipid monolayers at the air-water interface and on solid supports*. Thin Solid Films, 1988. **159**: p. 17-28

[9] G. H. Wu *et al.*, *Interaction between lipid monolayers and poloxamer 188: An X-ray reflectivity and diffraction study*. Biophysical Journal, 2005. **89**(5): p. 3159-3173

[10] Pedersen, J.S. and Hamley, I.W. *Analysis of neutron and x-ray reflectivity data by constrained least squares methods*. Physica B, 1994. **198**(1-3): p. 16-23

[11] Nagle, J.F. and Tristram-Nagle, S. *Structure of lipid bilayers*. Biochimica et Biophysica Acta, 2000. **1469**(3): p. 159-195

[12] Sun, W.J. *et al. Order and disorder in fully hydrated unoriented bilayers of gel phase dipalmitoyl phosphophatidylcholine.* Physical Review E, 1994. **49**(5): p. 4665-4676

[13] Miller, C.E. *et al., Part I: An x-ray scattering study of cholera toxin penetration and induced phase transformation in lipid membranes.* Biophysical Journal, 2008. **95**(2): p. 629-640

[14] Sun, W.J. *et al., Strucutre of gel phase saturated lecithin bilayers: temperature and chain length dependence.* Biophysical Journal, 1996. **71**(2): p. 885-891

[15] Miller, C.E. *et al., Characterization of biological this films at the solid-liquid interface by x-ray reflectivity.* Physical Review Letters, 2005. **94**(23): 238104

[16] Tristram-Nagle, S. *et al., Structure of gel phase DMPC determined by x-ray diffraction.* Biophysical Journal, 2002. **83**(6): p. 3324-3335

[17] Tristram-Nagle, S. *et al., Measurement of chain tilt angle in fully hydrated bilayers of gel phase lecithins.* Biophysical Journal, 1993. **64**(4): p. 1097-1109

[18] Kjaer, K. *Some simple ideas on X-ray reflection and grazing-incidence diffraction from thin surfactant films.* Physica B, 1994. **198**(1): p. 100-109

[19] Katsaras, J., Yang, D. S. C., and Epand, R.M. *Fatty-acid chain tilt angles and directions in dipalmitoyl phosphatidylcholine bilayers.* Biophysical Journal, 1992. **63**(4): p. 1170-1175

[20] Ignes-Mullol, J. *et al. Spread monolayers: Structure, flows and dynamic self-organization phenomena.* Physics Reports, 2007. **448**(5-6): p. 163-179

# CHAPTER III

# Membrane Texture Induced by Specific Protein Binding and Receptor Clustering: Active roles for lipids in cellular function

E. B. Watkins[*, †], C. E. Miller[†, ‡], J. Majewski[†], T. L. Kuhl[§, ¶]

[*] Biophysics Graduate Group, University of California, Davis, 95616, USA
[†]Manuel Lujan Neutron Scattering Center, Los Alamos National Laboratory, Los Alamos, New Mexico, 87545, USA
[‡]Stanford Synchrotron Radiation Lightsource, Menlo Park, California, 94025, USA
[§]Department of Biomedical Engineering, University of California, Davis, California, 95616, USA
[¶]Department of Chemical Engineering and Material Science, University of California, Davis, California, 95616, USA

## *Abstract:*

Biological membranes are complex, self-organized structures that define boundaries and compartmentalize space in living matter. Composed of a wide variety of lipid and protein molecules, these responsive surfaces mediate transmembrane signaling and material transport within the cell and with its environment. It is well known that lipid membrane properties change as a function of composition and phase state, and that protein-lipid interactions can

induce changes in the membrane's properties and biochemical response. Here, molecular level changes in lipid organization induced by multivalent toxin binding were investigated using grazing incidence x-ray diffraction. Structural changes to lipid monolayers at the air-water interface and bilayers at the solid-water interface were studied before and after specific binding of cholera toxin to membrane embedded receptors. At biologically relevant surface pressures, protein binding perturbed lipid packing within monolayers and bilayers resulting in topological defects and the emergence of a new orientationally textured lipid phase. In bilayers this altered lipid order was transmitted from the receptor laden exterior membrane leaflet to the inner leaflet, representing a potential mechanism for lipid mediated outside-in signaling by multivalent protein binding. It is further hypothesized that cell surface micro-domains exhibiting this type of lipid order may serve as nucleation sites for vesicle formation in clathrin independent endocytosis of cholera toxin.

## *Introduction:*

Interactions between proteins and the cell membrane are an integral aspect of many biological processes[1]. Diverse protein-lipid complexes exist including transmembrane proteins, peripheral membrane proteins, and proteins bound to membrane associated receptor molecules. The interplay between these biological components is multifaceted: lipids can influence the structure and function of membrane proteins and at the same time membrane proteins can impact lipid organization [2]. In model systems lipids are capable of adopting a

variety of different ordered states with their phase behavior primarily governed by steric and van der Waals interactions between neighboring head groups and alkyl chains. Their organization ranges from the tightly packed gel phase to the fluid like liquid ordered ($L_o$) and liquid disordered ($L_d$) phases. Lateral heterogeneities within model membranes due to the coexistence of $L_d$ and $L_o$ phases have been widely used to study lipid domain formation and as analogs for lipid rafts [3, 4]. In biological systems, lipid rafts are dynamic self-organized membrane microdomains that selectively recruit specific proteins and lipids while excluding others [5, 6]. Typically enriched in cholesterol, sphingolipids, and glycolipids, rafts are characterized by the tighter packing of their constituent molecules in a liquid ordered phase [7]. Raft microdomains offer a means to sequester proteins, enhance the local concentration of raft associated components, as well as alter the conformation of embedded proteins within the cellular membrane. Another example of membrane microdomains is the self association of glycosphingolipids (GSL) to form a glycosynapse. Such microdomains are thought to play a role in a wide range of biological functions including cell recognition, adhesion, and signaling [8, 9]. For example, in cell adhesion processes GSL-GSL interactions directly influence membrane properties and GSL microdomains modulate the activity of protein kinases. A structural mechanism has not yet been established to explain how GSL microdomains modify cellular activity. In rafts, lipid induced protein conformation changes can also influence signaling by membrane embedded protein receptors, e.g. ion-channel linked receptors, enzyme linked receptors, and G protein coupled receptors (GPCR), as they transmit signals across the

membrane (outside-in signaling) through conformational or chemical changes to the protein's intracellular domain upon small molecule binding to an extracellular domain. This may, for example, open a channel, activate enzymatic activity, or induce a signaling cascade that results in a cellular response. However, to our knowledge a "lipid only" mediated structural mechanism for transmembrane signaling has not yet been reported. In the work reported here, we examine if the modulation of lipid membrane by specific protein binding can provide a potential mechanism for transmembrane signaling.

Cholera toxin, which selectively binds to ganglioside glycolipids, is frequently used as a reporter for membrane rafts and as a tool to investigate protein-lipid interactions [10]. The B subunit (CTB) is responsible for binding the toxin with highest affinity to ganglioside GM1 ($4.61 \times 10^{-12}$ M), a cell-surface receptor also associated with lipid raft domains [11]. Five identical B subunits, each containing one binding site, form a pentameric ring with a vertical height of 32Å and a radius of 31Å [12, 13]. Since binding is multivalent and of high affinity, off rates of the toxin are slow and the CTB-GM1 complex is very stable. This enables CTB to effectively cross-link GM1 receptors in the membrane. Receptor cross-linking, in general, may act to stabilize rafts, lead to coalescence of raft domains and is hypothesized to be involved in the exploitation of clathrin independent endocytosis pathways by multivalent toxins [14] Moreover, limiting the number of active binding pockets on cholera toxin has been shown to inhibit endocytosis, presumably due to diminished receptor cross-linking [15]. A mechanistic explanation for this phenomenon remains unclear.

Here we report the discovery of a new lipid phase generated by multivalent protein binding to raft associated membrane receptors. The packing characteristics of this *textured* lipid phase ($L_T$) place it intermediate between the well established $L_o$ and gel lipid phases. Not restricted to close packed structures, the $L_T$ phase comprises a rich variety of lipid orientations including anisotropic and azimuthally swirled lipid arrangements analogous to those observed in macroscopic hexatic phases of liquid crystals. Specific binding of protein to membrane embedded receptors was shown to generate the $L_T$ phase in model membranes, providing a possible window into otherwise undetectable features of lipid order within nanoscale domains in the cellular membrane. We propose that such orientationally textured domains may have biological relevance as lipid based signaling platforms and in cellular trafficking pathways. Significantly, these altered packing arrangements are transmitted from the receptor laden leaflet to the inner leaflet of the membrane providing a means for outside-in signaling. In addition, the $L_T$ phase offers a mechanistic explanation for non-clathrin mediated endocytosis where altered lipid packing due to toxin binding serves as a nucleation site for vesicle formation.

# Results:

### *Perturbations to lipid order in monolayers at the air-water interface*

To investigate the influence of multivalent protein binding on lipid order, phase state, and membrane texture, grazing incidence x-ray diffraction (GIXD) measurements were carried out on mixed DPPE:GM1 monolayers at the air-water

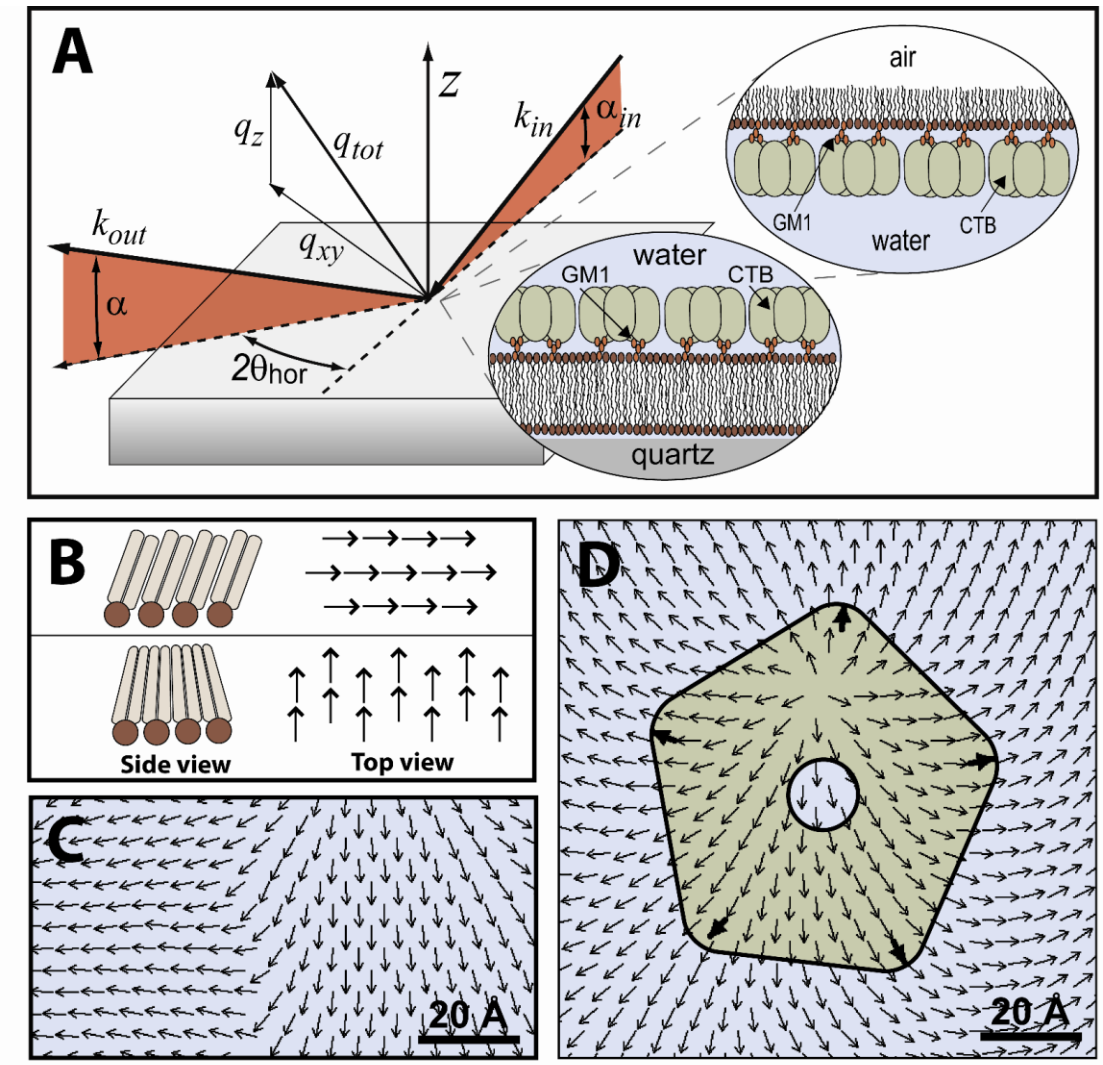


**Figure 1:**

**(A)** The GIXD scattering geometry is shown with schematic insets representing the monolayer and bilayer lipid-CTB systems studied.

**(B)** Tilt directors are vectors pointing along the lipids' alkyl chain backbones from the head group to the methyl end.

**(C)** A boundary between two orientations of the lipid tilt director field.

**(D)** Perturbation to the lipid tilt director field and associated topological defect induced by pentavalent binding of a single CTB protein.

interface in the presence and absence of CTB. Surface pressures spanned the range typically taken as the equivalent to a cellular membrane. GIXD restricts the scattering volume probed to the near surface region and is specialized for the investigation of in-plane order within thin, 2-dimensional films (Fig. 1A). Using this technique, we precisely characterized the packing of gel phase lipids and subsequent perturbation and disordering induced by protein binding. With sufficient GM1 receptors in the monolayer, high coverage 2-D cholera protein layers were assembled [16, 17]. On a local scale, this model system is analogous to nanoscale protein aggregates and provides the advantage of amplifying the scattering signal. Reflectivity measurements were used to confirm the formation of a bound protein layer [16]. Additionally, reflectivity showed that protein did not penetrate into the lipid monolayer after binding to GM1. Thus, the observed perturbations to lipid order originate from geometric constraints originating from multivalent binding and protein aggregation rather than protein penetration into the lipid layer.

Diffraction from ordered systems of long linear amphiphilic molecules like phospholipids is traditionally described as originating from arrangements of close packed rod-shaped molecules (alkyl chains) in 2-D hexagonal or distorted hexagonal unit cells [18, 19]. These molecular arrangements, typical of lipid monolayers in the gel phase, consist of uniformly oriented molecules with constant tilt magnitude and azimuthal tilt direction (Fig. 1B). Tilt directors, which are vectors pointing along the alkyl chain backbones of the lipid molecules, can be used to define their orientational order. Gel phase monolayers have a uniform tilt director field with all vectors aligned (Fig. 1C). Variations in the orientation of

the molecular tilt directors due to protein binding introduce texture and topological defects into the tilt director field (Fig. 1D). Such orientational texture in lipid packing has recently been reported both at the micron and molecular scales [20, 21]. Using models with close packed rod-shaped molecules and uniform tilt director fields, we parameterized the lipid order within the monolayer at three surface pressures and distortions resulting from protein binding.

Contour plots of diffracted intensities as a function of photon momentum transfer provide a convenient means to visualize diffraction from 2-D lipid films. Fig. 2A shows diffraction from a 80:20 DPPE:GM1 monolayer at 45mN/m surface pressure. The single degenerate peak at low $q_z$ (momentum transfer normal to the interface) indicates hexagonal packing and little molecular tilt of the hydrocarbon tails. In the presence of CTB the diffraction peak shifts slightly to lower $q_{xy}$ (momentum transfer along the interface) and higher $q_z$ corresponding to a small increase in lipid alkyl chain tilt and the area per lipid molecule (APM). At 30mN/m (Fig. 2B), the diffraction before protein binding is qualitatively similar to 45mN/m and, again, protein binding further increased lipid tilt and APM. In this case the lipid tilt upon protein binding is sufficiently large to clearly resolve the splitting of the degenerate peak into three distinct reflections indicative of a distorted hexagonal unit cell. We further comment that for these higher surface pressure cases, the changes in APM observed were commensurate with increased lipid tilt and conservation of the cross sectional area of the hydrocarbon chains. This shows that at high surface pressure the geometric constraints imposed by multivalent protein binding increase the

magnitude of molecular tilt and influence the positional ordering of hydrocarbon chains in the lipid monolayer.

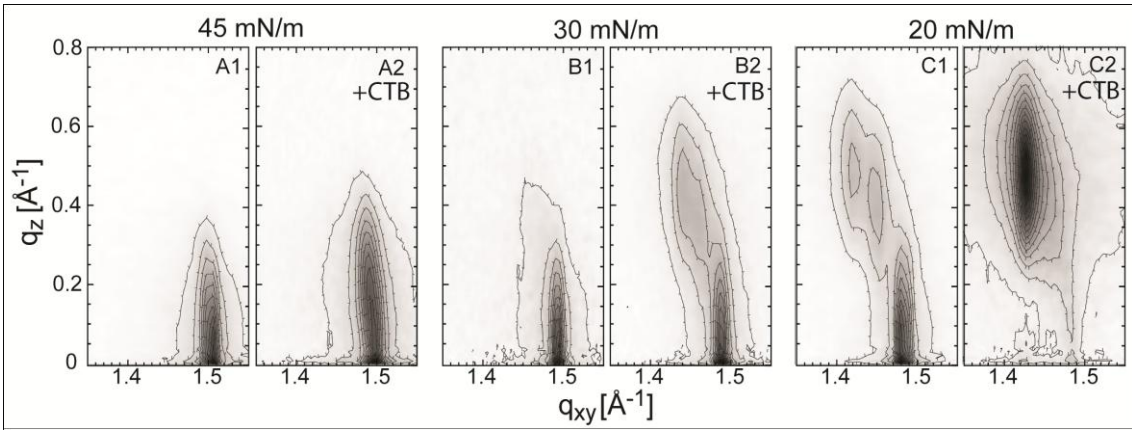


**Figure 2:**
Grazing incidence diffraction from 80:20 DPPE:GM1 monolayers at three surface pressures (A1,B1,C1) and diffraction from the same systems following binding of CTB (A2,B2,C2). At high surface pressures, protein binding causes an increase in the lipid APM that is commensurate with the increase in lipid tilt. Although APM increased after CTB binding at 20mN/m, the lipid tilt remained approximately the same. The resulting lipid order was no longer close packed and exhibited topological defects and texture of the lipid tilt orientations.

Very different diffraction is observed at a biologically relevant surface pressure (20mN/m) upon protein binding. The lipid diffraction in the absence of protein exhibits three non-degenerate peaks from an oblique unit cell (Fig. 2C). Protein binding, however, induces perturbations to the lipid order that greatly reduce the diffraction intensity at low $q_z$. The diffraction is still consistent with an increase in the APM but in this case the diffraction cannot be attributed to a simple increase in lipid tilt and a concomitant change in positional order. Moreover, the scattering can no longer be described by any model based on close packed cylindrical molecules and a uniform tilt director field. The necessary

relationships between both the diffraction peak positions ($q_{z_{q_z1}}^{max} = q_{z_{q_z2}}^{max} + q_{z_{q_z3}}^{max}$) and peak intensities ($I_1$=$I_2$=$I_3$) required for close packed molecular arrangements are violated [22]. In order to reduce the low $q_z$ intensity and match the measured diffraction, topological defects and orientational texture have to be introduced into the lipid tilt director vector field (Fig. 1D). These changes represent the emergence of a new textured lipid phase, $L_T$, induced by multivalent protein binding. The details of this new phase and modeling are described in the next section.

***Modeling GIXD from textured phase monolayers***

To describe lipid order in the textured $L_T$ phase, we implemented models that perturbed the lipid order away from a close-packed gel phase and calculated the associated diffraction. By loosening the constraint imposed by close packing of lipid alkyl chains, topological defects and orientational texture could be incorporated into these models. The diffraction pattern of a 20 mN/m monolayer prior to protein binding was reproduced with a uniformly oriented tilt director field. After protein binding, no close packed model was able to reproduce the diffraction pattern. Instead, a textured 2-D liquid crystal smectic-like phase, the new lipid $L_T$ phase, with azimuthal perturbations to the molecular tilt directors was required. The simplest texture, for example, can be generated from a single defect, or disclination, at the domain center. This yields an arrangement of tilt directors analogous to bend domains in liquid crystals [23]. Azimuthal angles of

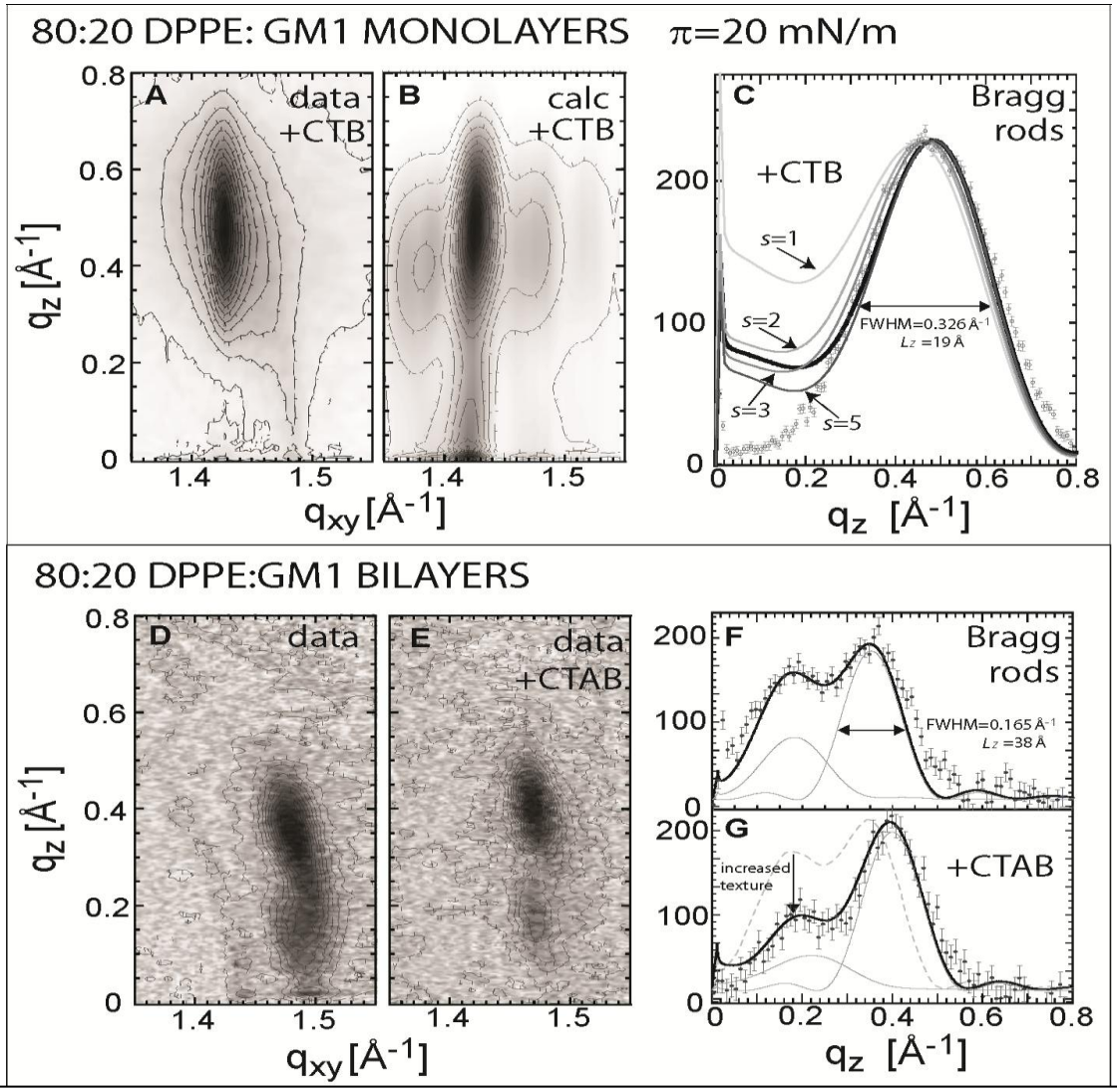


**Figure 3:**
Grazing incidence diffraction from monolayers with bound CTB (top) and bilayers before and after CTAB binding (bottom). Diffraction data from the monolayer-CTB complex (A) was reproduced by a textured lipid phase obtained *via* Monte Carlo simulation (B). Panel C shows fits to the Bragg rod extracted from (A) corresponding to single topological defect textures of different strengths ($s$=1,$s$=2,$s$=3,$s$=5) and to the Monte Carlo generated domain. For a domain radius of 150 Å (corresponding to the measured Bragg Peak FWHM), the scattered intensity at low $q_z$ decreased with increasing $s$. The best fit to the data was found for $s \approx 5$. In the bilayer case prior to protein binding (D,F), the Bragg rod FWHM indicates coupling between the membrane leaflets and exhibited limited texture. Following protein binding (E,G), cross leaflet coupling was preserved and the decreased intensity at low $q_z$ reflects an increased degree of texture.

the tilt directors were described by the equation $\phi = s \tan^{-1}(y/x) + \phi_0$ where $x$ and $y$ are the lateral coordinates of the molecules, and $s$ is the strength of the disclination with $s = \pm 1$ corresponding to the lowest energy, symmetric textures. The $L_T$ regions have a finite size and the average length scale associated with these domains is inversely related to the width of the Bragg peaks. For a domain radius of 150 Å (corresponding to the measured Bragg peak FWHM), the scattered intensity at low $q_z$ decreased with increasing $s$ until $s \approx 5$ (Fig. 3). Increasing the strength of the texture beyond this value did not improve the quality of the fit.

While diffraction from textured domains with a single center defect approximated the measured data, protein crystallography of the CTB-GM1 complex shows that bound GM1 molecules orient radially outward at an oblique angle from the protein's binding pocket [24]. Using additional Monte Carlo simulations we investigated how these geometrical constraints would influence the orientation of tilt directors and lipid order. Simulations of pentavelent CTB binding to 150 Å lipid domains that take into the geometric constraints imposed by the structure of the lipid-protein complex yielded highly textured tilt director fields containing multiple topological defects (Fig. 4). Diffraction patterns calculated from these lipid orientations were very similar to diffraction from domains with a single $s = 3$ disclination (Fig. 3). Using this more physically relevant model, the experimental diffraction data after CTB binding was best approximated by the scattering calculated from textured lipid phases with a molecular tilt magnitude of 20.0°, and an APM of 44.7 Å$^2$. Compared to the 20mN/m monolayer diffraction before protein binding, the tilt is unchanged and

the small 3.7% increase in APM (43.1 to 44.7 Å$^2$) corresponds to the degree that the lipid molecules are non-close packed. The modest APM expansion and loosened packing, driven by geometric constraints on the receptor molecules due to protein binding, indicates transformation to the $L_T$ phase.

***Perturbations to bilayer order induced by protein binding***

Bilayer studies allow the impact of multivalent protein binding on both leaflets to be investigated. GIXD experiments were conducted on DPPE:GM1 supported bilayers in the presence and absence of CTAB (Fig. 3 D-E) [25]. For simplicity, lateral correlations between tilt director orientations (Fig. 4) were not considered in these models. Prior to protein binding the lipids had an APM of 41.3 Å$^2$, were tilted 13.5° from the surface normal, and had a small degree of orientational texture. Molecular tilt directors spanned an azimuthal range with FWHM=22° resulting in a texture similar to the lipid order previously observed in supported phosphocholine bilayers [21]. Following protein binding, the lipid APM and tilt increased and the azimuthal variation increased to span a range with a FWHM=30°. Thus, the geometric constraints induced by protein binding decreased lipid packing efficiency and enhanced orientational texture in the bilayer in a manner similar to that observed with monolayers. Importantly, these lipid packing changes were transmitted across the bilayer - from the exterior leaflet containing GM1 receptors to the inner lipid leaflet. The coupling between the outer and inner membrane leaflet is clearly evident from Bragg rod peak width analysis. The FWHM in the Bragg rod intensity distribution relates to the

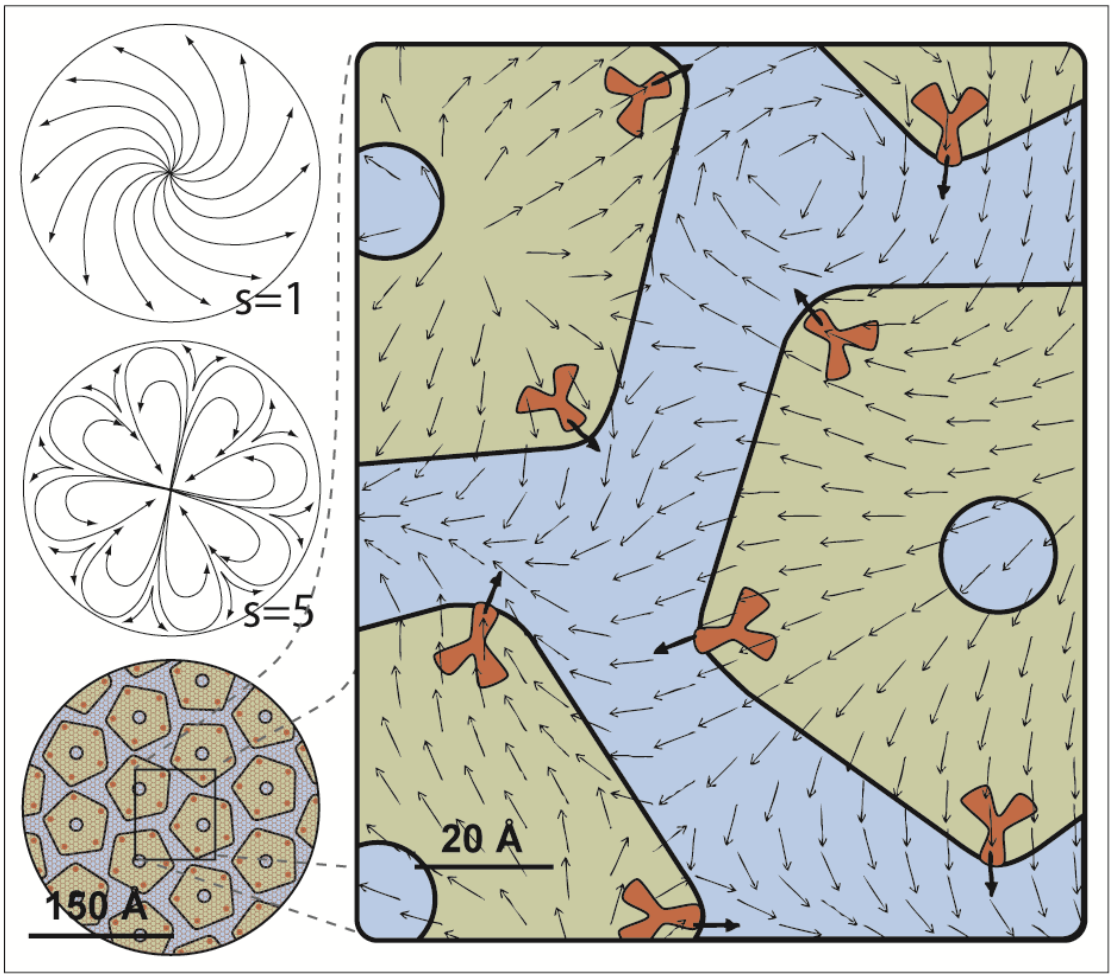


**Figure 4:**
Real space configurations of lipid tilt directors (vectors along the molecular backbones) exhibiting texture. Top left and middle schematics show orientation of tilt directors around an s=1, $\phi_0=\pi/4$ and an s=5, $\phi_0=\pi/4$ disclination respectively. In the bottom left schematic, ~10-15 CTB proteins are arranged beneath a 150 Å radius nano-domain corresponding to the lateral correlation size determined from the FWHM of the Bragg Peak. Magnification to the right displays the orientation of tilt directors obtained from MC simulation. Dark arrows represent molecules with fixed orientations. A topological defect can be seen near the central pore of the top left CTB molecule.

length of the diffracting lipid molecule. Assuming a rod-shaped scattering object the length over which the lipids diffract is given by the simple equation: FWHM=$2\pi/L_Z$. In the bilayer diffraction (Figure 3 F and G), the FWHM analysis yielded a length of about 40Å, twice the length of a lipid tail, and clearly demonstrates that the alkyl chains are coupled between the two leaflets both before and after protein binding. This molecular level coupling, which persists in the presence of cholera toxin, allows the perturbations to lipid order in one leaflet to be communicated to the opposing leaflet. Cross leaflet coupling of macro-phase separated membrane domains has been previously observed in model and cellular membranes and molecular level coupling has recently been reported in gel phase phosphocholine bilayers [21, 26, 27].

# Discussion:

### *Membrane topological defects and orientationally textured lipid phases*

We have observed that multivalent proteins can dramatically manipulate their lipid environment upon binding to their putative cell surface receptors. The protein does not penetrate the membrane, but imposes geometric constraints which restrict the position and orientation of bound receptors. At high lipid packing densities (high surface pressures), the perturbations to lipid order manifest themselves as changes in the lipid area per molecule (APM) and tilt magnitude. At lower surface pressures, protein binding changes the lipid tilt director field introducing topological defects and orientational textures. A

prerequisite for the formation of defects and textures is the relaxation of positional registry away from a close packed configuration. These structural changes due to protein-lipid complex formation reflect a phase transition from hexatic to a textured lipid phase, $L_T$, when the surface pressure is in a biologically relevant regime.

Orientational textures of lipids are analogous to larger length scale textures observed in liquid crystal systems and represent a newly identified lipid, $L_T$, phase state. This $L_T$ phase is characterized by molecular order intermediate between the gel and liquid ordered phases. Adjacent lipids cooperatively self-organize to accommodate receptors constrained by protein binding causing the emergence of textured domains. High surface pressures likely suppress the phase transition either by changing GM1's conformation or limiting the number of bound GM1 receptors. It is interesting to note that a natural consequence of the constrained orientation of bound receptors is the localization of topological defects at or near the position of CTB's central pore. In our Monte Carlo simulations this was observed in ~50% of the cases. Since cholera toxin's active A subunit attacks the membrane through CTB's pore, a topological defect and associated instability of the lipid packing in this region of the membrane should enhance translocation of the protein across cellular membranes.

The textured, $L_T$, phase and resulting topological defects may be prevalent in a variety of toxin-receptor membrane complexes featuring multivalent binding or nanoscale protein aggregation. For example, preliminary GIXD measurements indicate orientational texture in lipid monolayers following the binding of botulinum toxin. The crystal structure for this protein also suggests

that the ligand fits into the receptor's binding pocket at an oblique angle [28]. Although botulinum only has a single receptor site, protein aggregation and oligomerization may impose sufficient constraints to induce texture formation, similar to pentavalent cholera toxin binding.

### *Structural evidence for a non-clathrin mediated endocytosis pathway*

Cholera toxin's infection pathway involves transport of the protein across the plasma membrane followed by trafficking to the endoplasmic reticulum. Approximately half of the uptake of cholera molecules into cells is attributed to caveolar or clathrin mediated pathways and half is associated with GM1 enriched lipid rafts [29]. Raft associated endocytosis is driven by membrane dynamics and involves the formation of tubular structures with a diameter of 40-80nm and the creation of vesicles as a vehicle to transport the protein across the membrane [29]. Similar membrane invaginations have been correlated with the uptake of Shiga toxin, another pentavalent protein, and with simian virus 40 (SV40) both of which bind to raft associated glycolipids [30, 31] In the case of SV40, endocytotic uptake of the capsid was found to depend on GM1's tail structure and was enhanced when bound to GM1 with long saturated alkyl chains. The mechanism by which toxin binding initiates the formation of invaginations is unresolved. We propose that the generation of orientational texture induced by multivalent binding and protein aggregation initiates this process. Theoretical work has previously demonstrated that membrane regions incorporating textured domains can impact local membrane curvature and serve as nucleation

sites for the budding of vesicles [32]. Our studies show that multivalent protein binding to membrane receptors in both monolayers and bilayers generates the textured $L_T$ phase. Formation of texture through cooperative lipid rearrangement would be enhanced by long saturated alkyl tails, consistent with findings that endocytosis of SV40 is dependent on GM1's hydrocarbon structure. Our results are also consistent with the decreased internalization of cholera toxin when the number of active binding sites is reduced from 5 to 1-2 [15]. Such mutants retain their ability to bind and associate with lipid rafts but cannot cluster or cross link GM1 molecules as effectively. Mechanistically, these studies suggest that the formation of textured lipid micro-domains *via* multivalent binding and protein aggregation into clusters are important in triggering the endocytotic pathway.

### *A potential lipid mediated signaling mechanism*

Generation of orientational texture and a distinct $L_T$ lipid phase in membranes may have broad biological implications if perturbations to lipid order can be appropriated as a signaling mechanism by the cell. Analogous to $L_o$ / $L_d$ coexistence phases or self-association of order forming species in lipid rafts, textured lipid phases allow for new types of lateral heterogeneity in membranes. In addition, orientationally textured domains provide a means for protein binding induced changes in lipid order to be spread laterally by cooperative self-organization of adjacent lipids. Resulting alterations of membrane structure may facilitate raft clustering and potentially influence protein function (e.g. peripheral or transmembrane) at distant locations [4]. On a more local scale, textured lipid phases are also capable of transmitting information across the membrane. We

have shown that an extracellular molecule binding to membrane embedded receptors alters lipid packing and orientation within the receptor leaflet causing a phase transition to the $L_T$ phase and that these changes in packing and orientation are transmitted to the opposing leaflet. The resulting structural changes do not require either the translocation of a small signaling molecule through the membrane's hydrophobic core or the transmission of the signal *via* conformational or chemical changes to a transmembrane protein. Rather, if we consider the bilayer as an analog to a cellular membrane the altered lipid order at the apical leaflet induces a change in the packing of the cytoplasmic leaflet. This represents the possibility for a fundamentally new, lipid mediated mechanism for transmembrane signal transduction.

## *Experimental Section:*

### *Materials*

Lipid monolayers and bilayers were composed of 80:20 mole % of DPPE: GM1 [1, 2-Dipalmitoyl-*sn*-Glycero-3-Phosphoethanolamine: Galactosyl-N-Acetylgalactosaminyl (N-acetyl-neuraminyl) Galactosylglucosylceramide (GM1 Ganglioside)] from Avanti Polar Lipids. Although limited in physiological relevance to the exoplasmic leaflet, DPPE satisfies the conditions for diffraction and bears structural similarities to a large variety of saturated phospholipids, sphingolipids, and ceramides present in cellular membranes. Previous work has shown that DPPE and GM1 are miscible and do not phase separate under these

conditions. Lipids were dissolved in chloroform:methanol 90:10 (~1mg/mL) and deposited on an $H_2O$ pH=8 buffered subphase prepared using Millipore water with 170 mM NaCl, 1.4 mM Sodium Azide, 0.3mM EDTA, 15mM Trizma-Base from Sigma. The cholera toxin CTAB and subunit CTB were purchased from Sigma. For monolayer experiments, CTB in powder form was dissolved in water and injected into the subphase to a final concentration of ~4 mg/L. High receptor concentration in the monolayer and high protein concentration in the subphase yielded 2-D protein crystals bound to the monolayer with surface coverage ~50-60% [16]. Surface pressure of the monolayer was adjusted from 20 to 45mN/m and the temperature was 23°C. Bilayer samples were deposited *via* Langmuir-Blodgett and Langmuir-Schaffer deposition technique at 45mN/m and incubated with a 0.1 mg/ml CTAB solution for a minimum of 5 h before replacement with buffer.

### *Grazing incident X-Ray diffraction*

Synchrotron x-ray measurements on monolayers were carried out using a temperature controlled Langmuir trough mounted on the liquid surface diffractometer at the BW1 beam line at HASYLAB, DESY (Hamburg, Germany) at a wavelength of $\lambda$ = 1.304 Å. Soller collimation yielding a lateral resolution of $\Delta q_{xy}$ = 0.0084 $Å^{-1}$ and a one-dimensional position sensitive detector (PSD) with vertical acceptance $0 < q_Z < 1.2$ $Å^{-1}$ were used. Bilayer measurements were conducted on beamline 6-ID at the Advanced Photon Source (Argonne National Laboratory) at a wavelength of $\lambda$=0.545Å and data was collected using a Mar345

image plate. The high x-ray energy used enabled measurements to be performed at the solid-liquid interface through a 1cm thick water layer [21, 33]. For GIXD experiments, the x-ray beam was adjusted to strike the surface at an incident angle corresponding to momentum transfer vector $q_Z$ = 0.85 $q_C$, where $q_C$ is the critical scattering vector for total external reflection from the interface. At this angle an evanescent wave is generated which travels along the surface and Bragg scatters from the molecular arrangements at the interface.

## *Supplementary Information:*

### *Textured lipid phases*

We have observed that geometrical constraints imposed by multivalent protein binding and the aggregation of bound protein leads to the formation of topological defects and orientational texture in model biological membranes. A prerequisite for the formation of topological defects and textures is the relaxation of positional registry away from a close packed configuration. The additional positional freedom allows the molecules to adopt a richer variety of tilted orientations including anisotropic and azimuthally swirled lipid arrangements. Such arrangements of molecular orientations can be defined by vector fields composed of individual molecular tilt directors. Lipid organization of this type retains hexatic positional order and the associated topological defects correspond to disclinations in the vector field representing molecular orientations. Although

it is possible that the topological defects in the tilt director field discussed are also centered on point defects in the lipid bilayer, this assumption is not required.

### *GIXD analysis of close packed molecular arrangements*

*$\pi$=45mN/m, 80:20 DPPE:GM1 before CTB binding*

At a surface pressure of 45 mN/m, diffraction from the lipid monolayer indicates a hexagonal unit cell with the Bragg peak was centered at $q_{xy}$=1.504 Å$^{-1}$ corresponding to a primitive 2-D unit cell with dimensions |**a**|=|**b**|=4.82 Å and $\gamma$=120.0° (Table 1). Assuming the monolayer consists of a 2-D powder of crystallites, the lateral coherence length can be calculated using $L_{xy} \approx 0.9(2\pi/FWHM_{q_{xy}})$. After correcting for instrumental resolution, the intrinsic FWHM of the peak in the $q_{xy}$ direction was 0.0133 Å$^{-1}$ corresponding to a coherence length of ~430 Å. Thus, each scattering domain consists of approximately 2,900 lipids and 700 receptors with an average area per molecule (APM) of 40.3Å$^2$. The intensity distribution of the Bragg rod was calculated analytically by approximating the lipid tails as tilted cylinders with constant electron density and length $L_z$. The form factor of a cylindrical molecule is a disk oriented normal to the long axis of the cylinder with a thickness of $2\pi/ L_z$ and the intersection of the form factor with the lattice reflections yields the Bragg rod profile. Using this method, we determined that the alkyl chains in the 45 mN/m monolayer were tilted $\theta$=8.0° from the surface normal in the direction of the nearest neighbor (NN). The cross sectional area of two alkyl chains was

calculated as $A_C$=APM*$cos(\theta)$=39.9 Å$^2$ which is consistent with previously obtained values.

*$\pi$=45mN/m, 80:20 DPPE:GM1 after CTB binding*

After protein binding, the diffraction peak position shifted to lower $q_{xy}$ indicating an expansion of the hexagonal unit cell with an APM of 40.9 Å$^2$. The lateral coherence length also decreased by approximately a factor of two and represents a domain consisting of roughly 750 lipids and 200 receptors. Bragg rod models indicate an 11.6° tilt magnitude and a direction 18° away from the NN. This modest increase in tilt is consistent with the APM change, yielding a calculated alkyl chain cross sectional area of 40.1 Å$^2$.

*$\pi$=30mN/m, 80:20 DPPE:GM1 before and after CTB binding*

Similar perturbations to lipid order following CTB binding were observed at 30 mN/m surface pressure. The APM prior to protein binding was 40.9 Å$^2$, slightly larger than at the higher pressure, and the size of the scattering domain was comparable to the 45 mN/m case. The molecular tilt was 8.7° from the surface normal in the NN direction. Again, this combination of tilt and APM corresponds to a physically reasonable $A_C$. Following protein binding, the degeneracy of the reflections was broken and three distinct Bragg peaks, corresponding to the {0,1}, {1,0}, and {1,-1} reflections, were observed. The resulting oblique unit cell had an APM of 42.6 Å$^2$ and ~260 Å coherence length.

Consistent with a physically reasonable $A_C$, molecular tilt increased to 18.8° and pointed 13° from NN.

*π=20mN/m, 80:20 DPPE:GM1 before CTB binding*

At 20 mN/m surface pressure, three Bragg peaks can be distinguished and indexed according to an oblique unit cell with an APM of 43.1 Å$^2$ in the absence of protein. The size of the scattering domain was significantly smaller than at higher pressures with an average lateral coherence length of ~300 Å corresponding to approximately 1,200 lipid and 300 receptor molecules. Bragg rod fitting yielded a molecular tilt of 21.1° from the surface normal with an azimuthal direction 13° from NN. Again, the molecular tilt and APM define a physically reasonable cross sectional area for two alkyl tails of $A_C$=40.2 Å$^2$.

*π=20mN/m, 80:20 DPPE:GM1 after CTB binding*

Unlike the cases previously discussed, diffraction from the protein-lipid complex at 20mN/m consisted of a single peak centered at $q_{xy}$ =1.433 Å$^{-1}$ and $q_z$=0.475 Å$^{-1}$ with no significant intensity on or near the horizon. Assuming the molecules are close packed, the lack of intensity at small $q_z$ values suggests that the alkyl chains are tilted with an azimuthal direction towards the next nearest neighbor (NNN). Molecular tilt breaks the degeneracy of the first order reflections resulting in three equal intensity peaks which obey the relationship $q_{z\_1} = q_{z\_2} + q_{z\_3}$ where $q_{z\_1}$ is the position of the maximum intensity of the highest $q_z$ peak. However, it is not possible to describe the observed diffraction as a

superposition of three peaks which obey this relationship. Another possibility is that the measured intensity distribution consists of contributions from two degenerate peaks and a third non-degenerate peak that exists at higher $q_z$ but is not observed. We were able to analytically model the measured intensity distribution with a 37.9° tilt from the surface normal and a Debye-Waller (DW) > 3 Å to suppress the peak at $q_z$=0.95 Å$^{-1}$. Assuming a hexagonal unit cell, the $q_{xy}$ position of the peak yields an APM of 44.4 Å$^2$. For this APM and tilt, the calculated cross-sectional area, $A_C$, is less than 35 Å$^2$ which does not match other values obtained for this system and is unphysical. Although a hexagonal lattice is a good first approximation, introducing tilt will distort the unit cell. If we assume that the lipid tails are arranged as close packed cylinders, then the tilt and tilt direction are linked to the in-plane lattice parameters. For molecules tilted in the NNN direction, the constraint $\tan\theta = q_z/q_{xy}$ yields a $q_{xy}$ position of 1.22 Å$^{-1}$ and an APM of 50.0 Å$^2$. This suggests a surprisingly large change to the unit cell parameters following protein binding but no other traditional model involving close packed cylinders was able to reproduce the data. Although this model is capable of reproducing the measured diffraction pattern, it necessitates some extreme changes to the monolayer, such as the dramatic restructuring of the unit cell and greatly magnified roughness indicated by the high DW value, which raise questions about its validity. Reflectivity measurements provide further evidence contradicting this model: increasing molecular tilt by 15 degree would result in a 3 Å decrease in the monolayer thickness which reflectivity measurements did not detect.

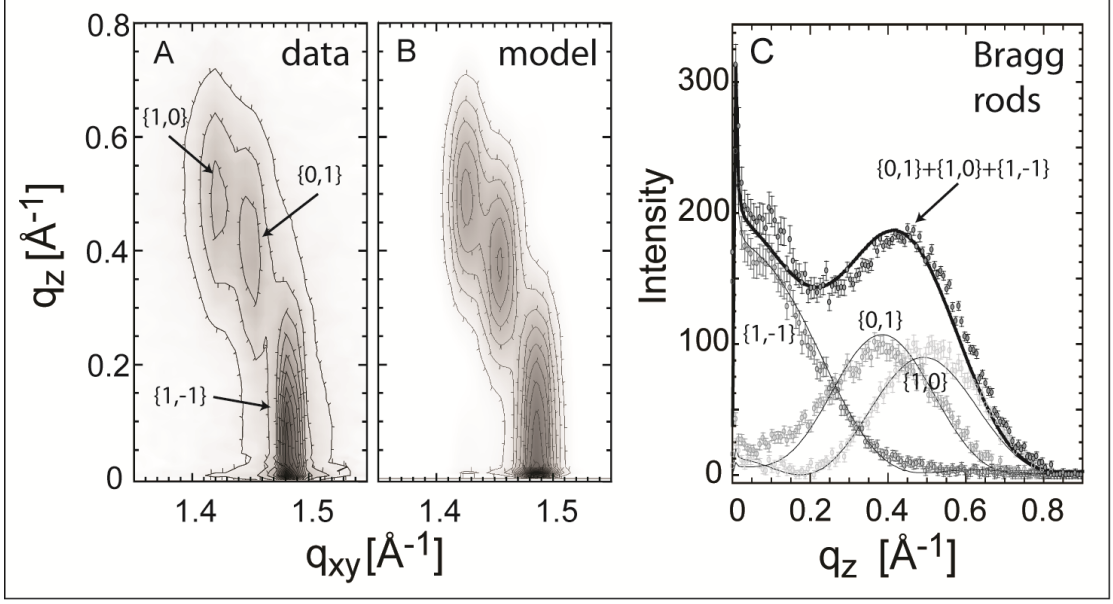


**Figure S1:**
Grazing incidence diffraction from 80:20 DPPE:$GM_1$ monolayers at 20 mN/m before CTB binding. For the unbound case, the data **(A)** can be modeled **(B)** by calculating the diffraction from a domain of azimuthally aligned lipids. Panel **(C)** shows the three individual Bragg rods extracted from the model calculation match the measured data.

***GIXD analysis of textured phase monolayers***

Models based on the arrangement of close-packed cylinder can not provide a satisfactory description of the diffraction from a 20 mN/m lipid monolayer after CTB protein binding. To fit the diffraction data from the lipid-CTB complex at 20mN/m, several attempts were made to develop non-close packed descriptions of the system including ones involving anisotropic perturbations to positional order, perturbations to the out of plane tilt magnitudes, and perturbations to the in-plane tilt directions. Only the last set of models, as described in this work, was successful in approximating both the $q_z$ and $q_{xy}$

intensity distributions. In contrast to modeling using the analytical form factor of a cylinder, we used a more flexible “beads on a line” approach to model non-close packed structures [16]. The alkyl tails were approximated as equidistant beads and the diffracted intensity was calculated discretely for given molecular orientations within the scattering domain. To describe the monolayer, sixteen beads, each representing a $CH_2$, were arranged on a 20 Å line and an end bead of each of these molecules was fixed to a hexagonal lattice. Using this method, the 20 mN/m monolayer diffraction pattern prior to protein introduction was reproduced with a uniformly oriented tilt director field and the parameters obtained from traditional analyses of the Bragg peak and rod (Fig. S1).

To describe the system after protein binding, textured 2-D liquid crystal smectic phases were created through azimuthal perturbations to the molecular tilt directors. Textured phases scatter less coherently as azimuthal disorder increases and, depending on the range of azimuthal angles, the individual Bragg reflections are effected differently. As a result, the multiplicity rule is broken and the relative intensities of the reflections are a result of geometry: i.e. as a tilted molecule changes its azimuthal direction the atoms move a greater distance perpendicular to one lattice plane as opposed to another. However, if the tilt directors sample all 360° of azimuthal angles, then the system is again rotationally symmetric and all reflections are contributed to equally.

From the diffraction pattern, one can not distinguish between random azimuthal disordering and arrangements where there is a correlation between the tilt director orientations of adjacent molecules but no preferred orientation in the overall domain. Although these systems diffract similarly, completely random

disordering would result in energetically unfavorable steric collisions. However, with a correlation between tilt directors of adjacent molecules and a sufficiently large domain the difference in the azimuthal angle between neighboring molecules will become vanishingly small and collisions will be eliminated. For the simplest possible set of models, the orientational texture originates from a single defect, or disclination, at the domain center and there are no discontinuity lines in the director field. This yields an arrangement of tilt directors analogous to bend domains in liquid crystals [17]. Azimuthal angles of the tilt directors are described by the equation $\phi = s \tan^{-1}(y/x) + \phi_0$ where $x$ and $y$ are the lateral coordinates of the molecules, and $s$ is the strength of the disclination with the lowest energy, symmetric textures being $s = \pm 1$. By changing the value of $\phi_0$, the director field can be altered to create sink, source, vortex, or anti-vortex textures. For a given disclination strength, all values of $\phi_0$ are energetically equivalent and the resulting calculated scattering patterns were qualitatively similar. Since we cannot distinguish between molecular arrangements on the bases of energetic favorability or scattered intensity, we modeled the diffraction from the protein-lipid complex as textured domains with center disclinations of varying strength and an arbitrary value of $\phi_0 = \pi/4$ . The texture strength, $s$, corresponds to the degree of orientational order within a domain. As the disclination strength is increased, the difference in azimuthal angle between neighboring molecules goes up and the domain becomes more disordered. The degree of disordering also depends on the size of the domain, with smaller domains requiring a larger difference in angle between neighbor molecules. Since the domain size can be

estimated from the scattered intensity's FWHM in $Q_{xy}$, the disclination strength can be adjusted to match the measured data. For a domain radius of 150 Å, the scattered intensity at low $q_z$ decreased with increasing $s$ until $s \approx 5$ providing the best match to the measured data.

***Table 1: GIXD structural parameters:***

| **80:20 DPPE: GM1** | $\pi$ (mN/m) | In-plane *Bragg Peaks* | | | | | Out-of-Plane *Bragg Rods* | | | |
|---|---|---|---|---|---|---|---|---|---|---|
| | | a (Å) ±0.01 | b (Å) ±0.01 | γ (°) ±0.4 | APM (Å$^2$) ±0.3 | $L_{xy}$ (Å) ±5.0 | $L_z$ (Å) ±5.0 | Tilt angle ±1.0 | Tilt dir. (from NN) ±2.0 | DW (Å) ±0.5 |
| Mono-layers | 45 | 4.82 | 4.82 | 120.0 | 40.3 | 430 | 19.3 | 8.0 ° | 0 ° | 2.0 |
| | 30 | 4.86 | 4.86 | 120.0 | 40.9 | 430 | 19.0 | 8.7 ° | 0 ° | 1.0 |
| | 20 | 4.89 | 4.99 | 117.9 | 43.1 | 300 | 19.6 | 21.1 ° | 13 ° | 1.6 |
| Mono-layers + bound CTB | 45 | 4.86 | 4.86 | 120.0 | 40.9 | 220 | 20.5 | 11.6 ° | 18 ° | 2.0 |
| | 30 | 4.88 | 4.95 | 118.4 | 42.6 | 260 | 18.5 | 18.8 ° | 13 ° | 1.3 |
| | 20 | 5.69<br>5.08* | 5.69<br>5.08* | 129.6<br>120.0* | 50.0<br>44.7* | 230<br>230* | 20.5<br>20.0* | 37.9 °<br>21.0 °* | 31 °<br>N/A* | 3.4<br>1.0* |

*Parameters obtained from $L_T$ calculations and not traditional Bragg peak and rod fitting.

***Monte Carlo simulations of multivalent cholera binding***

While diffraction from textured domains with a single center defect succeeded in approximating the measured data, there were no direct geometric connections to the structure of the lipid-protein complex. Inspection of the protein crystallography structure of the CTB-GM1 complex shows that the orientation of the receptor pockets orients the ligands such that they point radially outward and at an oblique angle from the protein's top surface. We investigated how these geometrical constraints influence the orientation of tilt directors and lipid order. To accomplish this, Monte Carlo simulations were implemented to generate domains which minimized the difference in the

orientation of neighboring tilt directors while maintaining no net tilt orientation of the overall domain. CTB molecules were arranged on a hexagonal lattice corresponding to the measured protein diffraction with a random azimuthal orientation of proteins. For each CTB, the azimuthal tilt directions of the five hydrocarbon chains nearest to the binding sites were fixed to point radially outward from the protein center. Hydrocarbon chains were then randomly inserted into free positions on the lattice adjacent to existing molecules until the domain was filled. Finally, two chains were randomly selected and, if determined to be energetically favorable, there tilt directions were swapped. The swapping routine was implemented for ~$1 \cdot 10^7$ iterations until a minimum energy state for the domain was obtained.

Monte Carlo techniques were also implemented to investigate the influence of binding valency on the formation of topological defects and orientational texture (Fig. S2). Experiments have show decreased internalization of cholera toxin when the number of active binding sites is reduced from 5 to 1-2 [10]. A reduction in binding sites would certainly limit the geometric constraints imposed by multivalent binding. However, monovalent binding would not impact the geometric constraints caused by the formation of nanoscale protein aggregates. To address this issue, we performed a series of Monte Carlo simulations to investigate the impact of binding valency on the formation of texture and topological defects. While pentavalent binding resulted in the highest defect density, a reduction to monovalent binding did not eliminate either the presence of topological defects or orientational texture. This suggests that both

multivalent protein binding and protein aggregation within lipid rafts may enhance vesicle formation and endocytotic uptake of the protein into the cell.

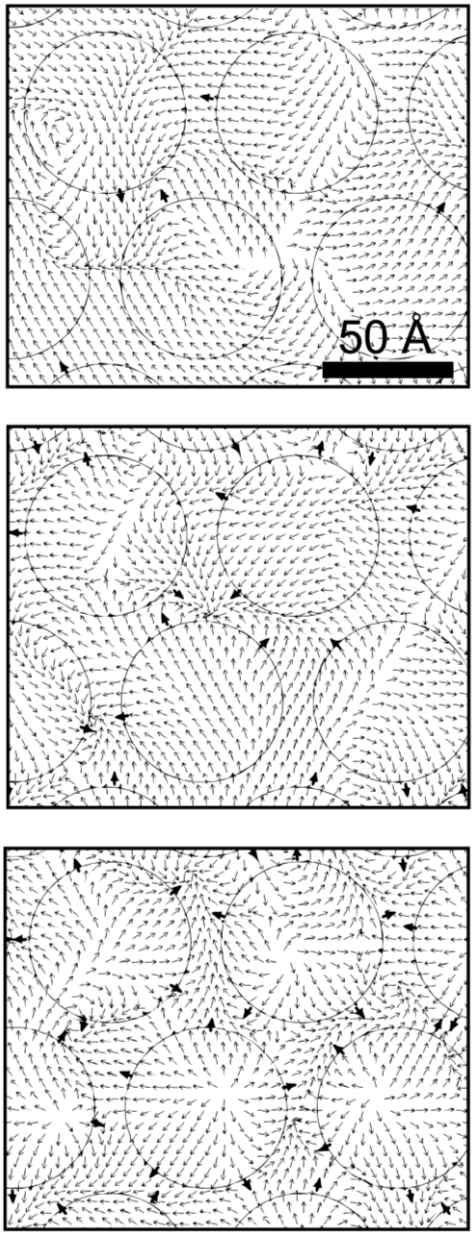


**Figure S2:**
Lipid tilt director fields obtained from Monte Carlo simulations at different binding valencies. From top to bottom, the director fields show the impact of monovalent, trivalent, and pentavalent binding on the formation of topological defects and orientational texture. Bound molecules are indicated by thick arrows.

## *Acknowledgements:*

This work was supported by the National Science Foundation Chemistry Division under award 0957868, the DOE Office of Basic Energy Sciences and Los Alamos National Laboratory under DOE Contract DE-AC52-06NA25396. TLK thanks the Jeff and Diane Child/Steve Whitaker fund for Distinguished Teaching and Scholarship for financial support. We thank Dr. Kristian Kjaer for help with the monolayer scattering and Dr. Doug Robinson for assistance with the bilayer measurements.

## *References*:

1. White, S.H. and W.C. Wimley, *Membrane protein folding and stability: Physical principles*. Annual Review of Biophysics and Biomolecular Structure, 1999. **28**: p. 319-365.
2. Phillips, R., et al., *Emerging roles for lipids in shaping membrane-protein function*. Nature, 2009. **459**(7245): p. 379-385.
3. Dietrich, C., et al., *Lipid rafts reconstituted in model membranes*. Biophysical Journal, 2001. **80**(3): p. 1417-1428.
4. Risselada, H.J. and S.J. Marrink, *The molecular face of lipid rafts in model membranes*. Proceedings of the National Academy of Sciences of the United States of America, 2008. **105**(45): p. 17367-17372.

5. Simons, K. and E. Ikonen, *Functional rafts in cell membranes*. Nature, 1997. **387**(6633): p. 569-572.

6. Edidin, M., *The state of lipid rafts: From model membranes to cells*. Annual Review of Biophysics and Biomolecular Structure, 2003. **32**: p. 257-283.

7. Lingwood, D. and K. Simons, *Lipid Rafts As a Membrane-Organizing Principle*. Science, 2010. **327**(5961): p. 46-50.

8. Hakomori, S., *The glycosynapse*. Proceedings of the National Academy of Sciences of the United States of America, 2002. **99**(1): p. 225-232.

9. Hakomori, S.I., *Structure and function of glycosphingolipids and sphingolipids: Recollections and future trends*. Biochimica Et Biophysica Acta-General Subjects, 2008. **1780**(3): p. 325-346.

10. Hammond, A.T., et al., *Crosslinking a lipid raft component triggers liquid ordered-liquid disordered phase separation in model plasma membranes*. Proceedings of the National Academy of Sciences of the United States of America, 2005. **102**(18): p. 6320-6325.

11. Kuziemko, G.M., M. Stroh, and R.C. Stevens, *Cholera toxin binding affinity and specificity for gangliosides determined by surface plasmon resonance*. Biochemistry, 1996. **35**(20): p. 6375-6384.

12. Zhang, R.G., et al., *The 3-Dimensional Crystal-Structure of Cholera-Toxin*. Journal of Molecular Biology, 1995. **251**(4): p. 563-573.

13. Zhang, R.G., et al., *The 2.4 Angstrom Crystal-Structure of Cholera-Toxin-B Subunit Pentamer - Choleragenoid*. Journal of Molecular Biology, 1995. **251**(4): p. 550-562.

14. Lundmark, R. and S.R. Carlsson, *Driving membrane curvature in clathrin-dependent and clathrin-independent endocytosis*. Seminars in Cell & Developmental Biology, 2010. **21**(4): p. 363-370.

15. Wolf, A.A., et al., *Attenuated endocytosis and toxicity of a mutant cholera toxin with decreased ability to cluster ganglioside GM(1) molecules*. Infection and Immunity, 2008. **76**(4): p. 1476-1484.

16. Miller, C.E., et al., *Part I: An x-ray scattering study of cholera toxin penetration and induced phase transformations in lipid membranes*. Biophysical Journal, 2008. **95**(2): p. 629-640.

17. Miller, C.E., et al., *Part II: Diffraction from two-dimensional cholera toxin crystals bound to their receptors in a lipid monolayer*. Biophysical Journal, 2008. **95**(2): p. 641-647.

18. Alsnielsen, J., et al., *Principles and Applications of Grazing-Incidence X-Ray and Neutron-Scattering from Ordered Molecular Monolayers at the Air-Water-Interface*. Physics Reports-Review Section of Physics Letters, 1994. **246**(5): p. 252-313.

19. Kjaer, K., *Some Simple Ideas on X-Ray Reflection and Grazing-Incidence Diffraction from Thin Surfactant Films*. Physica B, 1994. **198**(1-3): p. 100-109.

20. Bernchou, U., et al., *Texture of Lipid Bilayer Domains*. Journal of the American Chemical Society, 2009. **131**(40): p. 14130-+.

21. Watkins, E.B., et al., *Structure and Orientational Texture of Self-Organizing Lipid Bilayers*. Physical Review Letters, 2009. **102**(23): p. -.

22. Kaganer, V.M., et al., *Tilted Phases of Fatty-Acid Monolayers*. Journal of Chemical Physics, 1995. **102**(23): p. 9412-9422.

23. Ignes-Mullol, J., et al., *Spread monolayers: Structure, flows and dynamic self-organization phenomena*. Physics Reports-Review Section of Physics Letters, 2007. **448**(5-6): p. 163-179.

24. Merritt, E.A., et al., *Structural studies of receptor binding by cholera toxin mutants*. Protein Science, 1997. **6**(7): p. 1516-1528.

25. In this case the full toxin was used, but without enzymatic cleavage and activation of the A subunit the effects on lipid order can be attributed to binding of the B subunit only.

26. Collins, M.D. and S.L. Keller, *Tuning lipid mixtures to induce or suppress domain formation across leaflets of unsupported asymmetric bilayers*. Proceedings of the National Academy of Sciences of the United States of America, 2008. **105**(1): p. 124-128.

27. Lingwood, D., et al., *Plasma membranes are poised for activation of raft phase coalescence at physiological temperature*. Proceedings of the National Academy of Sciences of the United States of America, 2008. **105**(29): p. 10005-10010.

28. Stenmark, P., et al., *Crystal structure of botulinum neurotoxin type a in complex with the cell surface co-receptor GT1b - Insight into the toxin-neuron interaction*. Plos Pathogens, 2008. **4**(8): p. -.

29. Kirkham, M., et al., *Ultrastructural identification of uncoated caveolin-independent early endocytic vehicles*. Journal of Cell Biology, 2005. **168**(3): p. 465-476.

30. Romer, W., et al., *Shiga toxin induces tubular membrane invaginations for its uptake into cells*. Nature, 2007. **450**(7170): p. 670-U3.

31. Ewers, H., et al., *GM1 structure determines SV40-induced membrane invagination and infection*. Nature Cell Biology, 2010. **12**(1): p. 11-U36.

32. Sarasij, R.C. and M. Rao, *Tilt texture domains on a membrane and chirality induced budding*. Physical Review Letters, 2002. **88**(8): p. -.

33. Miller, C.E., et al., *Probing the local order of single phospholipid membranes using grazing incidence x-ray diffraction*. Physical Review Letters, 2008. **1**(5): p. -.

# CHAPTER IV

# Structure and thermodynamics of lipid bilayers on polyethylene glycol cushions: Fact and fiction of PEG cushioned membranes

E. B. Watkins[*], R.J. El-khouri[†], C. E. Miller[‡], B.G.Seaby[¥], C.M. Marques, J. Majewski[‡], T. L. Kuhl[¥¶]

[*] Biophysics Graduate Group, University of California, Davis, 95616, USA
[†] Department of Chemistry, University of California, Davis, 95616, USA
[‡]Manuel Lujan Neutron Scattering Center, Los Alamos National Laboratory, Los Alamos, NM, 87545, USA
[¥]Department of Chemical Engineering and Materials Science, University of California, Davis, 95616, USA
[Δ] Institut Charles Sadron, Université de Strasbourg, CNRS-UPR 22, Strasbourg, 67034, France
[¶] Department of Biomedical Engineering, University of California, Davis, 95616, USA

## *Abstract:*

In developing well hydrated polymer cushioned membranes, structural studies are often neglected. In this work, neutron and x-ray reflectivity studies reveal that hybrid bilayer-polyethylene glycol (PEG) systems created from mixtures of phospholipids and PEG conjugated lipopolymers do not yield a hydrated cushion beneath the bilayer unless the terminal ends of the

lipopolymers are functionalized with reactive end-groups and can covalently bind (tether) to the underlying support surface. While reactive PEG tethered systems yielded bilayers with near complete surface coverage, a bimodal distribution of heights with sub-micron lateral dimensions were observed consisting of cushioned membrane domains and un-cushioned regions directly on the support. The membrane fraction cushioned by the hydrated polymer can be controlled by adjusting the molar ratio of lipopolymer in the bilayer. A general phase diagram based on the free energy of the various configurations is derived that qualitatively predicts the observed behavior and the resulting structure of such systems *a priori*. As further evidenced by ellipsometry, atomic force and fluorescence microscopy, the tethered system provides a simple means for fabricating small cushioned membrane domains within a membrane.

## *Introduction:*

A long term goal for biophysical studies of membranes, transmembrane proteins and lipid-protein interactions has been to fabricate biomimetic membranes on solid supports. However, the proximity of the solid substrate results in detrimental interactions between the substrate and protein frequently leading to protein denaturing and limited protein mobility [1-3]. The extent to which lipid packing and membrane organization is altered by interactions with the support also remains unclear. A highly hydrated “cushion” between the membrane and the underlying solid support may alleviate these effects and allow

structural characterization of the membrane free from substrate interactions; their study under more biologically relevant conditions is, in many cases, a necessary prerequisite for the study of membrane proteins. To achieve this goal, a large research effort has been directed towards engineering polymeric cushions with beneficial properties [1-9]. However, structural characterization of cushioned membrane systems has been limited. This lack of information can potentially lead to misinterpretation of experimental data such as lipid and protein diffusion coefficients.

Due to its non-ionic nature and biocompatibility, polyethylene glycol (PEG) has become a commonly used platform for cushioning membranes [7, 10-13]. In this work, we investigated the structure of membranes supported by PEG lipopolymers. Two types of cushions were constructed: one with a reactive silane at the terminal end of the PEG to tether the lipopolymer to the underlying surface, similar to the system described by Tamm and coworkers, and the other lacking this reactive functionality [8]. Typically, fluorescent microscopy is used to characterize the homogeneity and fluidity of such hybrid systems. For example, membranes containing such lipopolymers can routinely be deposited to yield a uniform fluorescent field as

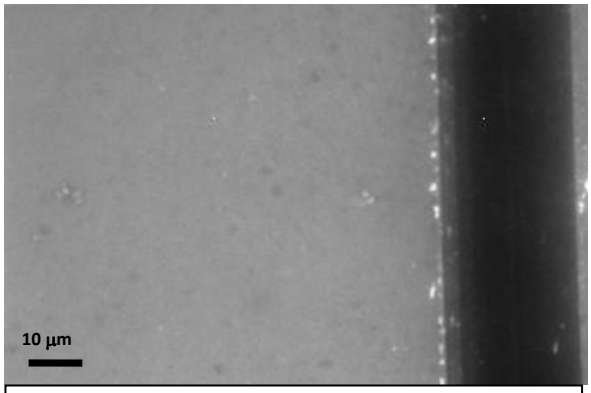


**Figure 1.** Fluorescent microscopy image of a DSPE-esPEG2k bilayer composed of 5 mol% lipopolymer and 2 mol% NBD-DPPE. The uniform field suggests the existence of a full coverage membrane without phase separation or lateral heterogeneities. The vertical dark line corresponds to a membrane region removed *via* scratching with tweezers.

shown in Figure 1. Indeed, many studies in the literature have used fluorescent microscopy to suggest incorporation of lipopolymers yields homogenously cushioned membranes [7, 10-13]. However, these results can be misleading and there has been little effort devoted to precise structural characterization of PEG membrane cushions. In this work, we use neutron and x-ray reflectometry as well as complementary techniques to investigate the structure and properties of several PEG membrane cushion preparations. We also provide a qualitative phase diagram that can be used to predict the resulting structure of such systems *a priori*.

## *Materials and methods:*

### *Materials and synthesis*

Figure 2A shows the chemical structure of the lipids used in the bulk of this work. All lipids were purchased from Avanti Polar Lipids (Alabaster, AL): 1,2-Distearoyl-*sn*-Glycero-3-Phosphoethanolamine (DSPE), 1,2-Distearoyl-*sn*-Glycero-3-Phosphoethanolamine-N-[Polyethylene Glycol-2000] (DSPE-PEG2k), 1,2-Distearoyl-*sn*-Glycero-3-Phosphoethanolamine-N-[Amino(Polyethylene Glycol)2000] (amine terminated DSPE-PEG2k), 1,2-dipalmitoyl-*sn*-glycero-3-phosphocholine (DPPC) and 1-palmitoyl-2-oleoyl-*sn*-glycero-3-phosphocholine (POPC). Single crystal quartz substrates with 3 Å r.m.s roughness were obtained from Mark Optics (Santa Ana, Ca) for x-ray reflectivity experiments and Institute of Electronic Materials and Technology (Warsaw, PL) for neutron reflectivity experiments. Prior to use, the quartz substrates were sonicated in chloroform,

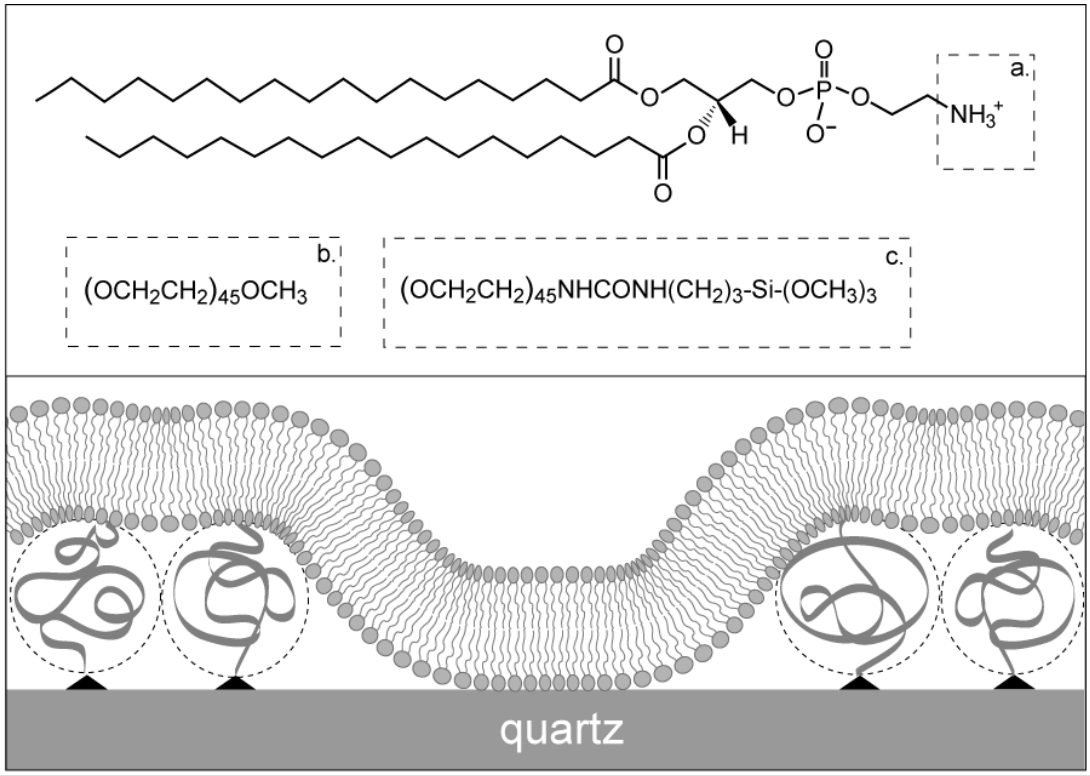


**Figure 2.** (Top) Molecular structure of (a.) DSPE, (b.) DSPE-PEG2k, and (c.) DSPE-esPEG2k with reactive ethoxy silane groups. Lipopolymer structures consist of the DSPE molecule with the contents of the corresponding dashed box substituted for the amine. (Bottom) Schematic of a bimodally distributed cushioned membrane formed with DSPE-esPEG2k.

Hellmanex soap solution, then rinsed in Millipore-deionized water and dried under a stream of pure Nitrogen ($N_2$). The substrates were then placed in a UV-Ozone chamber for 30-40 min. The cleaned substrates were water wetting, contact angle <10° as characterized via contact angle measurements.

An ethoxy silane terminated DSPE-PEG2k molecule (DSPE-esPEG2k) was synthesized from amine terminated DSPE-PEG2k and 3-(Triethoxysilyl)propyl isocyanate obtained from Sigma-Aldrich. These two components were mixed in a 1:1 ratio and the reaction was conducted in chloroform and stirred for at least 24h. Fourier transform infrared spectroscopy (FTIR) was used to measure loss of

isocyanate functionality and >98% conversion to the lipopolymer silane was obtained.

### *Sample preparation*

Bilayers were primarily prepared using the Langmuir Blodgett/Langmuir Schaeffer (LB/S) deposition technique. Lipids were dissolved at ~1.0 mg/ml in a 90:10 volume ratio chloroform and methanol mixture. For untethered PEG cushions, a 95:5 mole ratio of DSPE to DSPE-PEG2k was prepared and tethered PEG cushions were prepared from 98:2, 95:5, 93.5:6.5, 90:10 mole ratio DSPE:DSPE-esPEG2k mixtures. Spreading solutions were deposited onto a nanopure water subphase and solvent was allowed to evaporate. Monolayers were compressed to yield tightly packed lipid films (40-45 mN/m) and allowed to equilibrate before depositing. For DSPE-esPEG2k mixtures, the subphase was adjusted to pH~4 through the addition of HCl. Acidic conditions aid hydrolysis of the ethoxy groups, allowing polycondensation, and promote silane binding to hydroxyl groups on the quartz surface. For DSPE and DSPE-PEG2k mixtures, a 5-10 mm/min dip speed was typically used for depositing the inner leaflet. For DSPE-esPEG2k mixtures, a slower dip speed of 1mm/min was primarily used to facilitate ethoxy sliane coupling to the quartz surface. However, little difference was observed with this range of dip speeds. Most inner leaflets were allowed to dry for a few hours before the outer leaflet was deposited *via* Langmuir Schaeffer. In some cases, DSPE-esPEG2k inner leaflets were cured for 40 min at 70C before the outer leaflet was deposited. Little difference was observed in the absence of

the drying period or curing before deposition the outer leaflet (results not shown).

Bilayers incorporating reactive and non-reactive lipopolymer were also prepared using either DPPC or POPC matrix lipids *via* the vesicle fusion method. Thin films of dried lipids were dissolved at a concentration of 0.5 mg/ml in nanopure $H_2O$ and probe tip sonicated to yield small unilamellar vesicles. Vesicle solutions were immediately incubated with a clean quartz substrate for 30 min to allow fusion to take place before flushing with water. Additionally, a hybrid sample preparation technique involving an LB deposited inner leaflet and an outer leaflet deposited *via* vesicle fusion was investigated.

### *Neutron and X-ray reflectivity*

Reflectivity, *R*, is defined as the ratio of the number of particles (neutrons or photons) elastically and specularly scattered from a surface to that of the incident beam. When measured as a function of wave-vector transfer, $Q_Z = |k_{out} - k_{in}| = \frac{4\pi \sin\theta}{\lambda}$, where $\theta$ is the angle of incidence and $\lambda$ is the wavelength of the beam, the reflectivity curve contains information regarding the sample-normal profile of the in-plane averaged scattering length density (SLD) and is therefore most suited for studies of interfacial, layered films. From the measured reflectivity profile, the thickness, SLD, and roughness of a series of layers normal to the substrate can be determined by minimizing the difference between the measured reflectivity and that obtained from a modeled SLD profile [14].

Neutron reflectivity (NR) measurements were performed on the SPEAR beamline, a time of flight reflectometer, at the Manuel Lujan Jr. Neutron Scattering Center, Los Alamos National Laboratory. Using neutrons wavelengths $\lambda$=2-16 Å and two incident angles, values of the momentum transfer, $Q_z$, up to 0.25 Å$^{-1}$ and reflectivities down to $R \sim 5\times10^{-7}$ were measured. The coherence length of the neutron beam was of order 1 μm and the beam footprint was ~10x50 mm. Synchrotron x-ray reflectivity (XR) measurements were carried out at beamline 6-ID at the Advanced Photon Source (Argonne National Laboratory) at a wavelength of $\lambda$ =0.545 Å. The high x-ray energy used enabled measurements to be performed at the solid-liquid interface through a 1 cm thick water layer [15-17]. The footprint of the x-ray beam on the sample was ~1x10 mm. High photon flux, relative to the much lower neutron flux, allowed high resolution XR measurements up to $Q_z$ = 0.8Å$^{-1}$.

NR data was analyzed by minimizing the difference between the measured reflectivity profile and that calculated for a real-space model based on a series of layers describing the polymer cushioned membrane [18]. Using the Parratt formalism, box models described the SLD distribution as a sequence of *n* constant SLD layers. Error functions were used to connect adjoining layers and describe interfacial roughness. The higher momentum transfer vectors accessible in XR measurements allowed a model-free data fitting approach to be used where the electron density profile normal to the interface was constructed from a series of cubic B-splines [19]. The coefficients in the series of B-splines were determined by constrained nonlinear least-squares methods. We performed over a thousand refinements within the parameter space and present a family of models for each

reflectivity data set, all of which satisfy $\chi^2 \leq \chi^2_{minimum}+1$ with typical values of $\chi^2_{minimum} < 5$ [17]. Highly oscillating profiles, which were not physically reasonable, were excluded. Superimposing the accepted profiles yielded a broad electron density "ribbon" which is a measure of the uncertainty in the real space structure. Box models, consistent with the model-free ribbons, were also used to provide a more quantitative description of the system.

**Microscopy and ellipsometry**

Fluorescence microscopy images were taken on a Nikon Eclipse E600 microscope with 60X magnification water immersion lens. 1,2-dipalmitoyl-*sn*-glycero-3-phosphoethanolamine-N-(7-nitro-2-1,3-benzoxadiazol-4-yl) headgroup labeled fluorescent lipids (NBD-DPPE) were chosen to minimize perturbations to the alkyl chain packing. Samples incorporating 2 mol% NBD-DPPE were prepared by LB/S on quartz substrates and imaged in bulk water at room temperature.

Atomic Force Microscopy (AFM) was conducted using a Dimension 3100 Scanning Probe Microscope with a Hybrid closed-loop XYZ head and Nanoscope IVa controller (Vecco, Santa Barbara, CA). All samples were deposited on quartz substrates and imaged while submerged in nanopure water with a direct drive cantilever holder for fluids (Vecco, Santa Barbara, CA). A silicon nitride cantilever with a spring constant of 0.05 N/m was used at a scan rate of 0.5 Hz.

Ellipsometric angles and spatially resolved ellipsometric contrast images were acquired using a commercial Elli2000 imaging system (Nanofilm Technologie, Göttingen, Germany). Using a fluid cell, measurements under

aqueous conditions were taken at an incidence angle of 60°. Silicon substrates with a native oxide were used to enhance the optical contrast with the lipid phase. The specified accuracy in ellipsometric angle determination was 0.01°.

## *Results:*

To investigate the structure of PEG cushioned membranes, measurements of single component DSPE bilayers were compared to bilayers deposited from mixtures of DSPE and lipopolymer (DSPE with PEG polymer covalently bound to the head group, Figure 2). The terminus of the PEG chain was either a non-reactive methoxy group (DSPE-PEG) referred to as “non-tethered” or a reactive ethoxy silane group (DSPE-esPEG2k) referred to as “tethered”. Reactive ethoxy silane groups can form covalent bonds with the quartz substrate and cross-polymerize with each other, which should enhance the stability of the cushioned membrane. Based on previous literature a 95:5 mole ratio of 2,000 MW PEG conjugated DSPE lipids should yield a film where the PEG chains are in the overlapping mushroom regime [20-22]. The thickness of the cushion was therefore expected to be approximately 35 Å; the Flory radius of a PEG-2k chain. Higher and lower concentrations of PEG lipopolymer were also studied to investigate the impact of different PEG grafting densities on the structure and thickness of the cushion. Importantly, previous monolayer studies have observed no phase separation in lipid PEG mixtures at the air-water interface [22-24].

### *Neutron reflectivity*

*Pure DSPE*

We start with the reflectivity data and structure of a pure DSPE bilayer deposited on a quartz substrate (Fig. 3). Deuterated water was used to maximize the neutron scattering length density (SLD) contrast between the hydrogenated lipids and hydrated regions of the sample. With these contrast conditions, high SLD regions are attributed to water (and hydrated PEG cushion in subsequent studies of lipid and PEG lipopolymer mixtures), while SLD minima correspond to hydrocarbon containing regions of the lipid bilayer. Using the simplest, physically reasonable model we described the bilayer as a single homogenous layer of low SLD for the hydrocarbon tails with an additional layer to account for the hydrated cushion. Lipid head groups were not explicitly defined but can be approximated by interfacial roughness because they have an SLD intermediate between the lipid tail regions and either the quartz substrate or $D_2O$ superstrate. To further minimize fitting parameters, a 5Å r.m.s roughness was used at all interfaces which is typical for supported membranes [17, 25].

With this simple model, the structure of a DSPE bilayer was parameterized and fitted yielding a 45.0 Å thickness and a SLD of $-0.33 \times 10^{-6}$ Å$^{-2}$ (Table 1). For comparison, the maximum thickness in angstroms of a saturated hydrocarbon chain can be calculated theoretically using $l_{hc}=1.5+1.265\ n_c$ where $n_c$ is the number of carbons [26]. Thus, a DSPE bilayer has a theoretical maximum hydrocarbon thickness of 46.0Å. The fitted thickness matches closely, indicating that the lipid tails are oriented perpendicular to the substrate with little molecular tilt. From the thickness and measured SLD of the hydrocarbon layer

we obtain an average area per molecule of 38.2Å$^2$ which is consistent with gel phase PE lipids and indicates the presence of a well packed membrane with near complete surface coverage. This SLD profile for pure DSPE was used as a reference to calculate the membrane coverage for all other systems measured by NR presented in this work.

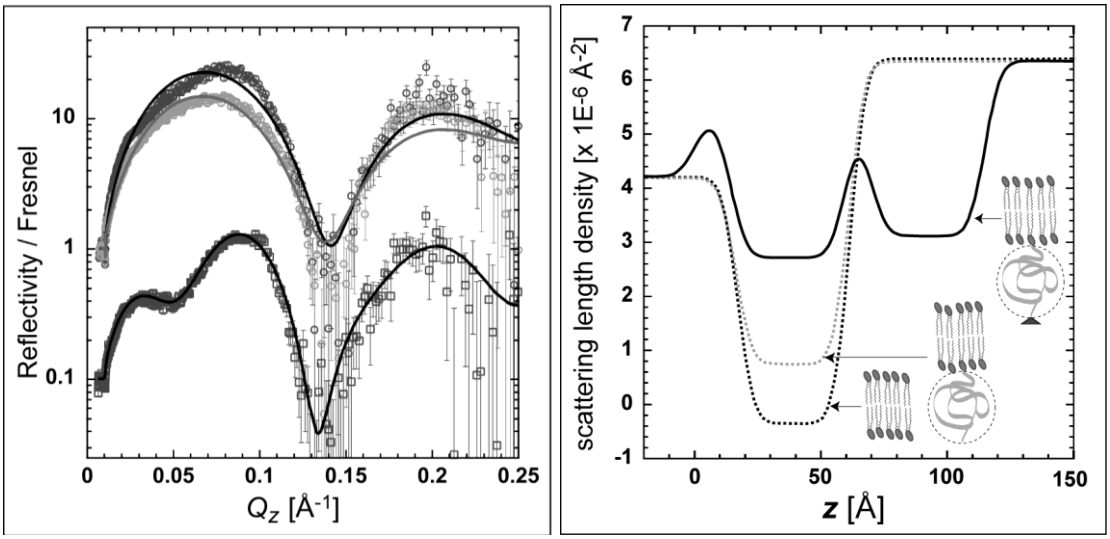


**Figure 3.** (Left) NR divided by Fresnel curve and fits: pure DSPE bilayer (top, dark), un-tethered 5 mol%DSPE-PEG2k bilayer (top, light), 5 mol% DSPE-esPEG2k tethered cushioned bilayer (bottom, shifted down for clarity). (Right) Lines represent box model SLD(z) corresponding to the reflectivities shown: pure DSPE bilayer (dark dashed line), un-tethered DSPE-PEG2k bilayer (light dashed line), and DSPE-esPEG tethered cushioned bilayer (solid line). The tethered, cushioned bilayer exhibits near complete coverage with approximately half the surface area on top of a thin hydrated layer adjacent to the quartz substrate and the other half supported by ~50Å of hydrated PEG cushion.

*5 mol% DSPE-PEG2k bilayers*

The neutron reflectivity profile of a supported DSPE bilayer containing 5 mol% un-tethered DSPE-PEG2k is very similar to that of the pure DSPE bilayer (Fig. 3). The minima are in the same positions indicating that the two samples

share the same length scales. The shapes of the fitted SLD profiles match, and the non-reactive PEG lipopolymer system's profile shows no evidence of either the lipid region shifting away from the quartz interface due to a PEG cushion or the presence of a second lipid minimum further away from the substrate. The main difference in the SLD profiles is the decreased height of the interference maxima of the DSPE-PEG2k mixture. Decreased interference maxima are due to reduced contrast of the layers, e.g. hydrocarbon tails and $D_20$, and indicate that this supported bilayer has either partial coverage or is less well ordered than a pure DSPE supported membrane. By assuming the average membrane structure consists of a linear combination of regions of well packed lipids and deuterated water, we calculate an 83% surface coverage for the 5 mol% DSPE-PEG2k mixed membrane. Fluorescent microscopy of the mixed membrane, however, shows a homogeneously fluorescent field indicating that the bare regions are sub-micron in size and cannot be resolved optically (Fig. 1). The low roughness of the mixed membrane (Table 1) extracted from modeling the reflectivity profile, is also consistent with small bare regions below the coherence length of the neutron.The changes in the reflectivity could not be modeled by preserving a high coverage bilayer and introducing a distribution of PEG above or below the bilayer. However, due to the low contrast between hydrated polymer and bulk water it was not possible to distinguish between two possible architectures: the absence of lipopolymer in a partial coverage bilayer and a partial coverage bilayer with PEG chains extending from the exterior leaflet. Due to this uncertainty, the DSPE-PEG2k system was modeled using a single layer to describe the lipid distribution and the PEG distribution was not explicitly included.

Several sample preparation parameters were adjusted in attempts to construct cushioned membranes including increased mole ratio of PEG conjugated lipids, increased PEG molecular weight, depositing the outer leaflet with and without drying and/or curing, replacing DSPE with a fluid phase matrix lipid, use of an ionic subphase, and employing different contrast conditions. In all of these cases a lipid membrane was obtained as evidenced by NR measurements; *however no PEG cushion was detected between the quartz and the supported membrane*. In addition, membrane preparation using vesicle fusion was found to yield similar results and did not show evidence of a PEG cushion. We emphasize the results from the more controlled LB/LS deposition method because more complete, less disordered membranes were formed using this approach.

*5 mol% DSPE-esPEG2k bilayers*

In contrast to solid supported DSPE and the un-reactive DSPE-PEG2k mixed membranes, reflectivity from membranes containing the reactive DSPE-esPEG2k system exhibit multiple minima representing more than one length scale (Fig. 3). Two distinct low SLD regions corresponding to the lipid hydrocarbon tails can be seen in the profile: one ~15 Å away and the other ~70 Å away from the quartz interface. Both regions are approximately 45 Å thick and represent a bimodal height distribution of the membrane. Based on the SLD profile, roughly half of the membrane is supported by a thin hydrated layer (15 Å) against the substrate and the other half is supported by a much thicker, hydrated PEG cushion (70Å). Assuming a homogenous distribution of PEG, a 5 mol% lipopolymer consists of weakly overlapping chains in the mushroom regime with

a predicted polymer layer thickness of 38 Å (approximately the Flory radius ($R_F$)) [21]. However, the measured PEG cushion thickness is significantly larger and indicative of an enrichment of lipopolymer in the cushioned regions. The rearrangement and segregation of lipopolmers conserves mass with half the membrane in contact with the underlying substrate and the other, cushioned half, enriched in lipopolymer by a factor of two. Qualitatively similar structures were measured for the same tethered system prepared after drying and curing, from mixtures with the addition of 5 mol% cholesterol, and from samples where the outer leaflet was deposited *via* vesicle fusion (data not shown).

Information about the lateral size distribution of the PEG cushioned and non-cushioned regions can also be gleaned from the NR measurements. Distinctly different reflectivity profiles would be measured depending on whether the in plane size of the cushioned regions is larger or smaller than the neutron coherence length (~1 μm). Beyond the coherence length, the reflectivity signal from the cushioned and non-cushioned regions will add incoherently, as a summation of distinct reflectivities from the two different regions. Instead, we observed that the membrane regions scatter coherently establishing that the cushioned membrane regions are smaller than the ~1 μm neutron coherence length.

*DSPE-esPEG2k bilayer concentration dependence*

In addition to 5 mol%, samples containing 2, 6.5, and 10 mol% DSPE-esPEG2k were measured (Fig. 4). At lower concentrations of DSPE-esPEG2k, bimodal distributions of the membranes were observed conserving the same

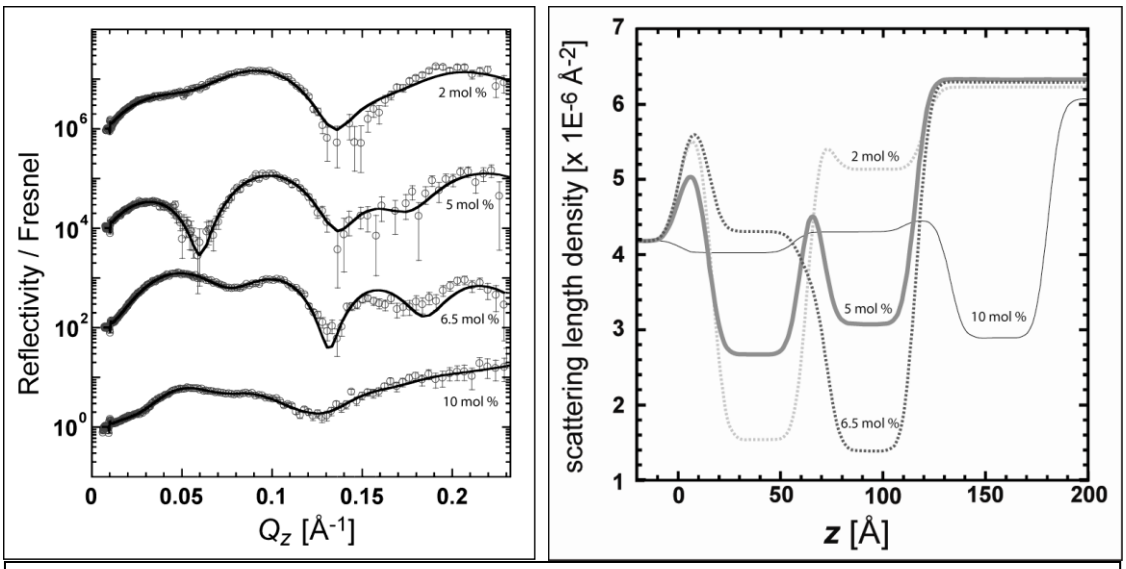


**Figure 4.** (Left) NR divided by Fresnel curve and fits of DSPE-esPEG2k cushioned bilayers with four different molar ratios of lipopolymer. Curves are shifted vertically for clarity by 100. (Right) Lines represent box model SLD*(z)* corresponding to the reflectivities shown. At lower molar ratios (2,5,6.5 mol%), there is a bimodal distribution of the bilayer with a greater fraction supported by the polymer cushion as the mole ratio increases. Above a critical point, the bimodal order breaks down and we observe a significant fraction of the membrane cushioned by a thicker and less well defined mixture of lipid, polymer, and water (10 mol%).

separation between the cushioned fraction of the membrane and the substrate. For the 2, 5, and 6.5 mol% mixtures, the cushioned fraction of the membrane was 0.26 ± 0.025, 0.52 ± 0.165 and 0.83 ± .02 respectively, showing a linear dependence of the cushioned fraction on the concentration of lipopolymer (inset Fig. 4B). Errors in the membrane's cushioned fraction were estimated by changing the corresponding SLD value while simultaneously allowing all other parameters to adjust until $\chi^2$ was increased by one. This linear trend did not continue at higher concentrations. Instead, at 10 mol% DSPE-esPEG2k, a trimodal distribution of heights was found with a new "cushioned" region detected about 130Å from the interface. The segregation of cushioned and non-

cushioned portions of the membrane suggests an equilibrium phase separation occurs. A model detailing this behavior is presented in the discussion section.

### *X-ray reflectivity*

To complement the NR measurements, we conducted X-ray reflectivity experiments at the solid liquid interface (Fig 5). Electron density profiles of solid supported pure DSPE bilayers demonstrate the advantages of higher resolution X-ray data. Features that cannot be resolved using NR, such as the low density methyl trough at the bilayer center, become well defined using X-rays. Consistent with the NR profiles, these measurements show a symmetric DSPE bilayer with near complete coverage that is conformal with the ~3 Å r.m.s quartz substrate.

XR also reconfirms the finding that the 5 mol% un-reactive DSPE-PEG2k systems do not yield cushioned membranes as the bilayers are directly supported by the quartz substrate (data not shown). Again, low contrast between hydrated polymer and bulk water prevented the determination of lipopolymer concentration in the exterior leaflet of the bilayer. Further, these systems exhibit a high degree of structural variability across a single sample indicating inhomogeneity and disorder in the bilayer but again no evidence of a cushioned membrane. Multiple samples were prepared including ones with a higher mole fraction of DSPE-PEG2k, increased PEG molecular weight, and the addition of cholesterol. For all cases, XR measurements did not detect a cushioned membrane.

XR data from the 5 mol% reactive or tethered PEG system is also consistent with neutron measurements. A bimodal distribution of the bilayer was

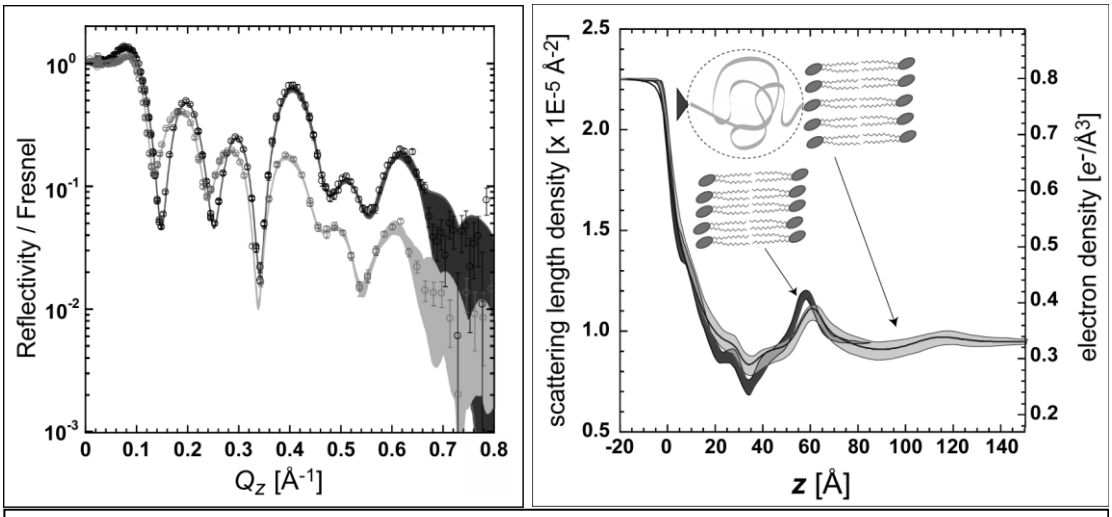


**Figure 5.** (Left) XR divided by Fresnel data and fits: pure DSPE membrane (dark) and a DSPE membrane containing 5 mol% reactive DSPE-esPEG-2k (light). (Right) Shaded curves show the family of SLD(z) fits within the selection criteria and $\chi 2=\chi min2+1$ corresponding to the reflectivities shown: DSPE bilayer (dark ribbon) and DSPE-esPEG-2k tethered, cushioned membrane (light ribbon). No cushion was observed for non-reactive, un-tethered PEG systems (data not shown). The solid line represents a box model to the DSPE-esPEG data and yields ~10Å r.m.s roughness for the cushioned bilayer.

observed with approximately half of the bilayer supported by a thin hydrated layer on the substrate and the other half resting on a thicker hydrated PEG cushion. Due to the lower roughness, the electron density profile of the membrane portion in closer contact with quartz is well defined and exhibits features similar to those observed for a pure DSPE bilayer. The total electron density profile in this region is an average of the supported bilayer and the hydrated PEG cushion. As a result, the electron density of the hydrocarbon tail region increased towards that of water while the electron density of the head group region was diminished. Electron densities obtained using box models indicate ~50% membrane coverage in contact with the underlying quartz substrate. A bump associated with the outer leaflet head groups and the

decreased electron density corresponding to the tails of the cushioned portion of the bilayer can be seen between 70 to 120 Å from the quartz surface. This is consistent with the membrane resting on a ~70 Å hydrated PEG cushion as found in the NR analysis. Despite the lower visibility compared to the quartz supported portion, box models indicate that approximately half of the membrane is supported by the PEG cushion with a 9 Å r.m.s. roughness. Since the primary electron density contrast in lipid bilayers measured in water is the electron rich head group and this region is a mere 10 Å thick, the deleterious effects of roughness on the measured structure are more apparent. Conversely, neutron contrast is derived from the 45 Å thick tail regions compared to $D_2O$ making the quality of that data less susceptible to roughness. Although the XR measurements had superior resolution, the combination of increased roughness and low electron density contrast of the cushioned system did not allow a more precise structural characterization than those based on NR measurements.

***Lateral structure***

Both ellipsometry and atomic force microscopy techniques were used to provide complementary information on the lateral structure of tethered PEG cushioned membranes. Ellipsometry measurements yielded an average film thickness of ~60 Å, consistent with the average thickness of the bimodal cushion observed using reflectivity. However, with a lateral resolution of 2 μm, micro mapping ellipsometry experiments were unable to resolve the lateral distribution of cushioned regions of the bilayer. Atomic force microscopy was therefore used to provide higher resolution images capable of resolving the lateral structure of

reactive PEG cushioned membrane (Fig. 6). The distribution of sample heights had a FWHM of ~35 Å and is consistent with the distance between the top surfaces of the solid supported and PEG cushioned bilayers. AFM shows that the cushioned regions of the membrane have sub micron dimensions as indicated by the reflectivity results. The cushioned regions again make up ~50% of the surface area and appear to be distributed fairly uniformly.

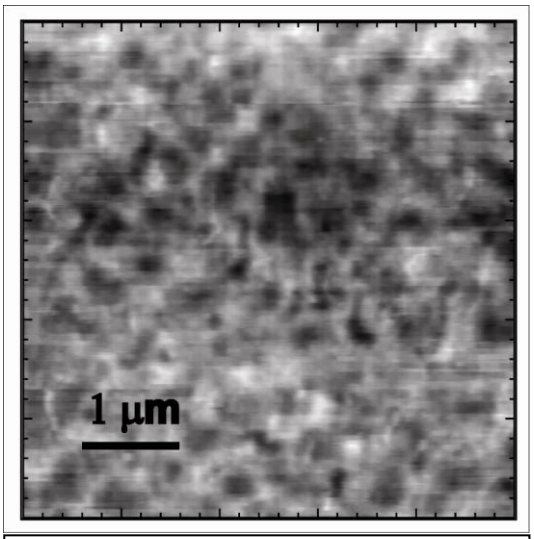


**Figure 6.** AFM image of a 5 mol% DSPE-esPEG2k tethered, cushioned bilayer. The FWHM of heights was ~35Å and lateral structure shows sub-micron domain sizes.

## *Discussion:*

### *Cushioned membrane structure*

The structure of PEG cushioned bilayers was investigated using neutron and x-ray reflectometry as well as complementary techniques to probe in-plane order. Previous work has suggested that a hydrated, PEG cushion could be prepared by incorporating unreactive PEG lipopolymers into the supported bilayer [7, 10-13]. Here we show that this approach does not yield a cushioned membrane whether vesicle fusion or the more controlled LB/LS deposition method is used. In all cases, there was no increase in distance between the membrane and support due to the presence of a PEG cushion and the membrane

formed is similar to that found in the absence of the lipopolymer. Indeed, the only difference in structure is that the membrane is more disordered when lipopolymer is incorporated. The absence of a cushion in these systems is also consistent with reported similarities in helical peptide diffusion within bilayers with and without non-reactive lipopolymers on a solid support [12].

A second, less commonly implemented method to construct cushioned membranes involves incorporating reactive lipopolymers into the membrane to enable covalent tethering of the terminal ends of the polymer to the substrate. A further feature is the potential for enhanced stability through polycondensation of the lipopolymers. This approach was pioneered by Tamm *et al* as a platform for studying membrane protein diffusion [4, 8]. Our structural characterization demonstrates that only portions of the bilayer are supported by hydrated cushioned regions with ~70 Å thicknesses. The remainder of the membrane is separated from the solid support by a thin hydrated layer. This bimodal distribution of the membrane heights maintains conservation of lipopolymer and is consistent with experimental measurements of protein diffusion. For example, lateral mobility of both cytochrome $b_5$ and annexin V in tethered lipopolymer supports was found to consist of two populations (referred to as mobile and immobile fractions) with different diffusion coefficients [8]. These observations may have less to do with intrinsic aspects of the proteins' diffusion in a cushioned membrane than with the bimodal distribution of the membrane itself. A similar bimodal membrane distribution for amino terminated PEG-lipids tethered to a COOH functionalized surface has recently been reported [27]. Based on XR measurements, it was suggested that this particular system yielded a mixture of

hydrated PEG and lipid micellular disks that cushion the membrane. Despite the higher resolution afforded by XR, the limited electron density contrast make x-rays less sensitive to the structure of lipopolymer assemblies than neutrons. Using NR, we observed that in all measurements of the reactive PEG systems the total surface area of both bilayer fractions approximates that of a full coverage membrane. Additionally, AFM measurements (Fig. 6) indicate height variations of the membrane surface commensurate with the bimodal distribution and also demonstrate that the two bilayer populations have sub-micron lateral domains sizes. However, these measurements cannot be used to determine the continuity of the bimodally distributed membrane.

To further understand the assembly of lipopolymer bilayers *via* the more controlled method of LB/LS, we investigated the structure of the inner leaflet following the first deposition. Deposited monolayers incorporating PEG lipopolymers exhibited a bimodal distribution of lipids and this structure was independent of tethering the polymer chains to the substrate *via* a reactive end-group. Neutron reflectivity from DSPE monolayers incorporating 5 mol% of either DSPE-PEG2k or reactive DSPE-esPEG2k was measured in $H_2O$ vapor (Fig. 7). In this case, lipids with deuterated alkyl tails were used and correspond to high SLD regions while SLD minima correspond to regions containing water and/or hydrated PEG cushion. For both non-reactive and tethered systems, box models indicate that the lipids are organized in a bimodal distribution following the first LB deposition. In this case, the bimodal distribution reflects regions of the monolayer in contact with the support (uncushioned) and regions on a PEG cushion ~35 Å from the interface. The thickness of the outer distribution of lipids

was intermediate between a monolayer and a bilayer. These measurements demonstrate that the monolayer structure is a precursor to the observed structure of the reactive, tethered bilayers and the bimodal distribution is not a consequence of the deposition of the outer leaflet. Since a similar bimodal distribution was not observed for un-tethered lipopolymer bilayers in bulk water, we hypothesize that in this case the deposition of the outer leaflet enables reorganization of the membrane. Energetic penalties arise from confinement of the lipopolymer between the substrate and the bilayer, hence in the absence of a reaction to the substrate, it is more favorable for the lipids to rearrange so that lipopolymer is exposed to bulk water. A significant portion of the bilayer may be damaged/removed during this reorganization, explaining the reduced coverage of bilayers containined untethered lipopolymer. When there is only a monolayer, it is unfavorable for the lipopolymers to rearrange.

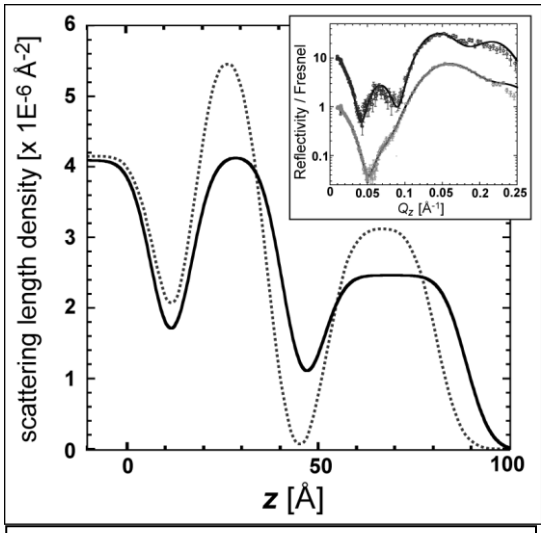


**Figure 7.** SLD(z) of deuterated lipopolymer monolayers in H2O vapor. Tethered (dark line) and un-tethered (dashed line) monolayers composed of DSPE and 5 mol % lipopolymer both exhibit a bimodal distribution of lipids. The inset shows corresponding NR data and fits.

### *Lipopolymer cushion thermodynamics*

The difference in membrane structure between non-reactive or reactive (tethered) lipopolymers can be further quantified using a straightforward

thermodynamic analysis of the free energy associated with the various system configurations. We consider two possible states for the phospholipid membrane containing a finite fraction of lipopolymers, as shown in Figure 8A: (1) a surface $S_1$ of the lipid bilayer is in direct contact with the underlying support, with all lipopolymers in the outer leaflet (uncushioned), and (2) a surface $S_2$ of the membrane contains lipopolymers in both leaflets, albeit with different surface densities (cushioned). Minimization of the free energy of the whole system with total fixed surface $S = S_1 + S_2$ determines the different surface fractions occupied by each state and the values of their corresponding lipopolymer densities.

The final equilibrium state of this system is controlled by two main parameters: the adhesion energy of the uncushioned membrane with the support, denoted by $\tilde{\varepsilon}$, and the interaction energy with the support of the end-functional group of the lipopolymer, denoted by $\tilde{\delta}$, where $\tilde{\delta} \approx 0$ for the non-reactive lipopolymer and $\tilde{\delta} >> 0$ for tethered chains. The excluded volume interactions between the polymers depend on the lipopolymer surface density $\sigma$: when the surface density is smaller than the overlapping concentration $\sigma << \sigma^*$, with $\sigma^* = 1/R_F^2$, chain-chain interactions are negligible. Above $\sigma^*$ excluded volume interactions can be accounted for by well-established polymer brush theories. The free energy of this generic system can thus be written as

$$F = S_1\left(k_B T A\left(\frac{\sigma_0}{\sigma^*}\right)^{5/6}\sigma_0 - \tilde{\varepsilon}\right) + S_2\left(k_B T A\left(\frac{\sigma_0}{\sigma^*}\right)^{5/6}\sigma_0 + k_B T A\left(\frac{\sigma_2}{\sigma^*}\right)^{5/6}\sigma_2 - \tilde{\delta}\sigma_2\right), \text{ Eq 1}$$

where $\sigma_o$ is the polymer density in the outer layer, $\sigma_2$ is the polymer density in the inner layer (for uncushioned membranes $\sigma_2 = 0$) and A is a constant of order

unity, $A \approx 1$. Equation (1) can be rewritten as a function of dimensionless quantities by using the following definitions: $x = S_1/S$, $(1-x) = S_2/S$, $\varepsilon = \tilde{\varepsilon}/(Ak_BT\sigma^*)$, $\delta = \tilde{\delta}/(Ak_BT)$, and by writing all surface densities $\sigma$ in units of $\sigma^*$ (i.e. $\sigma_0/\sigma^* = \tilde{\sigma}_0$). For simplicity, the tildes are dropped from the grafting density terms. This yields the free energy per unit surface as

$$\Im = \frac{F}{S} = k_BTA\sigma^*\left\{x\left(\sigma_0^{11/6} - \varepsilon\right) + (1-x)\left(\sigma_0^{11/6} + \sigma_2^{11/6} - \delta\sigma_2\right)\right\}, \text{ Eq 2}$$

Conservation of lipopolymer mass between $S_1$, $S_2$, and chains that may flip to the external leaflet requires $\sigma_0 x + (1-x)(\sigma_0 + \sigma_2) = 2\sigma$ or $x = \dfrac{\sigma_0 + \sigma_2 - 2\sigma}{\sigma_2}$.

Minimizing $\Im$ with respect to $\sigma_0$ and $\sigma_2$ gives the equilibrium values for these quantities. To make the algebra more tractable we first approximate the scaling exponent 11/6 by 2 and rescale the free energy per unit area to

$$f = \frac{\Im}{k_BTA\sigma^*} = \sigma_0^2 + x(-\varepsilon) + (1-x)\left(\sigma_2^2 - \delta\sigma_2\right), \text{ Eq 3}$$

Setting the partial derivatives to zero, $\dfrac{\partial f}{\partial \sigma_0} = \dfrac{\partial f}{\partial \sigma_2} = 0$, we find $\sigma_0 = \sqrt{\varepsilon} - \delta/2$, $\sigma_2 = \sqrt{\varepsilon}$, and $f_{\min} = -\dfrac{\delta^2}{4} - \left(2\sqrt{\varepsilon} - \delta\right)\left(\sqrt{\varepsilon} - 2\sigma\right)$. The equilibrium polymer densities are therefore a function of the adhesion energy $\varepsilon$ and of the sticking energy $\delta$. However, the set of solutions derived from Equation (3), where the two states coexist, only applies in a limited region of the full $\left[\delta, \sqrt{\varepsilon}\right]$ parameter space, depending on $\sigma$, the average polymer density per leaflet. The different possible

situations and the corresponding values of $\sigma_o$ and $\sigma_2$ are summarized in the state diagram shown in Figure 8B.

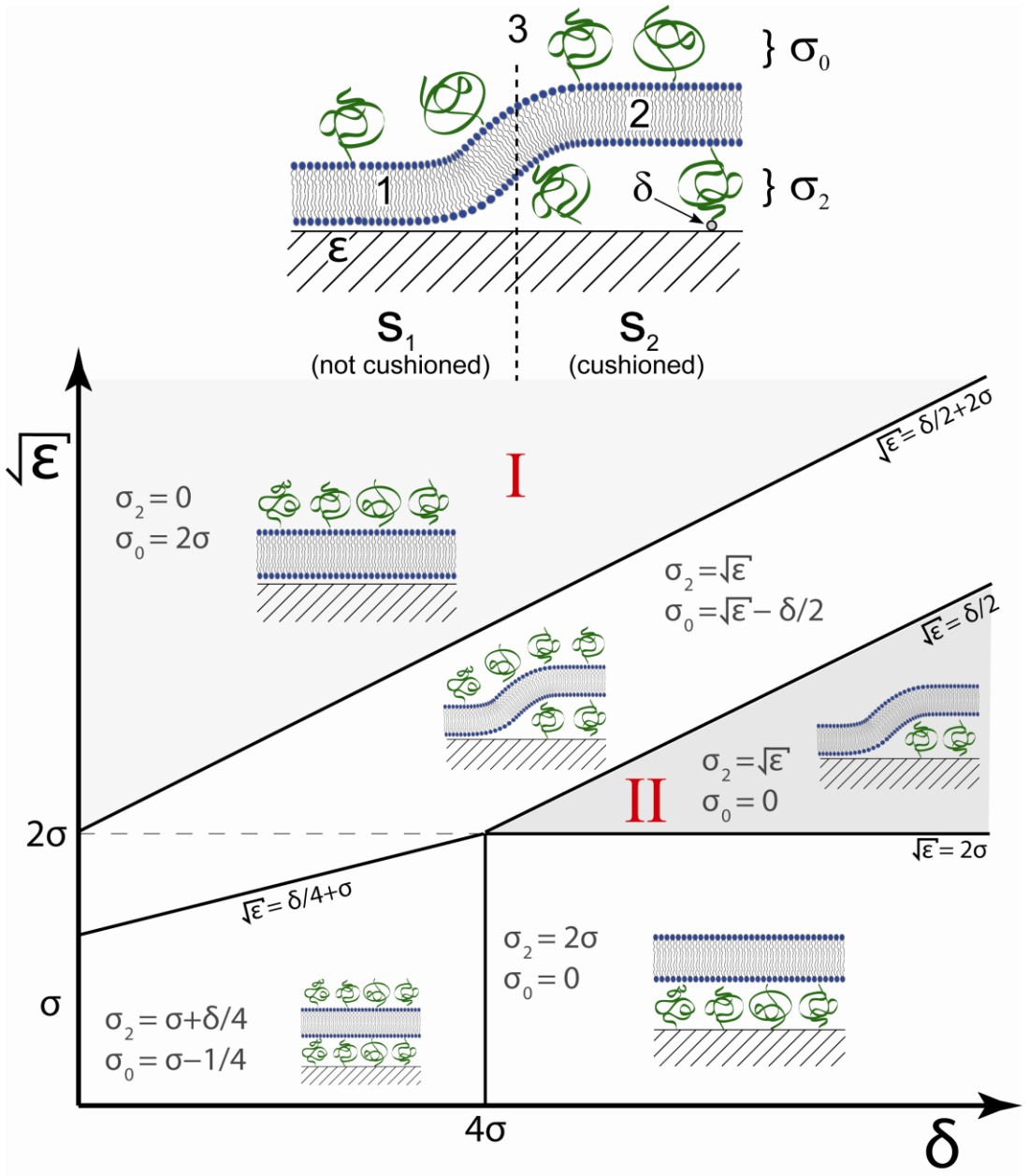


**Figure 8.** Phase diagram of various cushioned membrane states as a function of the membrane adhesion energy to the substrate, $\varepsilon$, the binding energy of the reactive group to the substrate, $\delta$, and the grafting density of the lipopoymers, $\sigma$. For the case of non-reactive lipopolymers $\delta \cong 0$ and $\varepsilon > 0$, the membrane system is in state I. In the reactive lipopolymer case, $\delta > 0$, however $\varepsilon$ is substantial and the membrane system is in state II.

The primary contributions to $\varepsilon$ are the van der Waals (VDW) and double-layer electrostatic interaction between the lipid membrane and the quartz support. The VDW energy between the substrate and a bilayer a distance *D* away can be approximated as [28]:

$$E_{VDW}(D) = -\frac{A_{123}}{12\pi D^2}$$

where the Hamaker constant $A_{123}$ is 7 x $10^{-21}$J [29]. The energy associated with VDW interactions is a significant contribution to the overall attraction of directly supported bilayers ($E_{VDW}(5\text{Å}) = -0.75 mJ/m^2$) but becomes negligible at the increased bilayer separations ($E_{VDW}(65\text{Å}) = -0.004 mJ/m^2$) of cushioned geometries [30]. Electric double-layer interactions yield an additional contribution to the energy that can be repulsive or attractive with asymmetric surfaces. To determine the electrostatic contribution for the various scenarios shown in Fig 8B, the double layer interactions were calculated by solving the nonlinear Poisson-Boltzmann equation explicitly using a numerical algorithm [31][32]. Given the low dielectric constant of the membrane's hydrocarbon core, we neglect the electrostatic contribution of any PEG-lipids in the outer leaflet of the membrane. The electrostatic interaction is always repulsive between the membrane and quartz under conditions of constant surface charge density. In contrast, when modeled under conditions of constant surface potential, the electrostatic interaction can be large and attractive between surfaces with a significant asymmetry in surface potential. Assuming quartz has a constant surface potential ($\psi_1$ = -50 mV), the contribution of electrostatic attraction is greatest for the case where the membrane is depleted of lipopolymers ($\psi_2 \rightarrow 0$) as

shown in Figure 9. Over a 4-6 pH range, the Debye length varies from 300-3000 Å, but only modestly impacts the electrostatic interaction for D<100 Å. Assuming a distance cut-off of 5 Å, the maximum electrostatic contribution is $\varepsilon \approx -2mJ/m^2$ for $\psi_1$ = -50 mV and $\psi_2$ = 0. Anderson and coworkers have recently reported measurements and similar modeling of the interaction of a phosphotidylcholine membrane supported on mica interacting with silica using the surface forces apparatus[33].

For comparison, we also model the electrostatic interaction for various lipopolymer membrane surface potentials (Figure 9). The surface potential of a membrane containing 5 mol% lipopolymer is negative and can vary from about -40 to -70 mV when the lipopolymer is dispersed in the membrane to -100mV within higher lipopolymer concentrations cushioned regions [34-37]. Only at small separations (D<40 Å) and very large surface potential differences is the electrostatic contribution for the cushioned system weakly attractive. At separations corresponding to the cushioned regions of the membrane, both the electrostatic interaction and VDW attraction are negligible, $\varepsilon \approx 0$. Thus, when the lipopolymer is non-reactive, $\delta = 0$, it is highly unfavorable for the

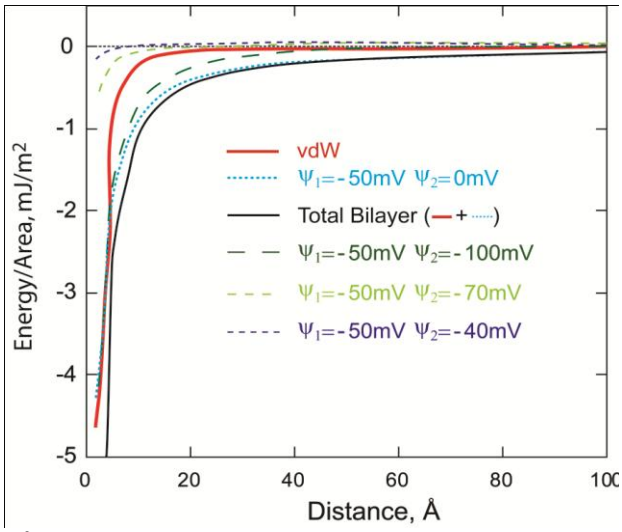


**Figure 9.**
Interaction free energy between a bilayer and quartz as a function of the bilayer surface potential.

lipopolymers to remain in the inner leaflet of the membrane, as the "bare" membrane-quartz interaction is more and more attractive as the membranes approaches the quartz and ($\psi_2 \rightarrow 0$). Consistent with our experimental measurements, regardless of non-reactive lipopolymer concentration the system reorganizes into state I of the phase diagram (Fig. 8B).

In contrast, incorporation of reactive lipopolymers yielded cushioned membranes in state II of the phase diagram. In regions where the membrane is supported on a PEG cushion, $\varepsilon \approx 0$, but the membrane is held to the quartz substrate given a sufficiently high binding energy between the reactive end-group and the substrate, $\delta > 0$. Silane coupling agents are known to bond well to quartz through hydrolysis of the ethoxy groups to silanols and subsequent polycondensation of these silanols and surface silanols [38]. With polycondensation of reactive lipopolymers and the energy of an Si-O bond being about 450 kJ/mole or 180 $k_BT$/bond, it is not surprising that $\delta >> 0$ and $\sigma_0 = 0$. However, concentrations of reactive lipopolymer $\leq 6.5\%$ always yielded a bimodal system of cushioned and non-cushioned regions (state II). Thus, we must also compare the contribution from polymer lateral interactions to $\varepsilon$, where at the minimum $\sigma_2 / \sigma^* = \sqrt{\varepsilon}$. We also note that the total PEG concentration was conserved in the inner leaflet and the cushioned regions in the bimodal system were enriched in PEG resulting in a cushion with an average thickness of about $2R_F$ (65 Å). The concentration of PEG in the cushion region corresponds to a PEG grafting density of about 1 PEG chain per 450 Å$^2$, or a concentration of 10 mol% PEG-lipid in the cushioned region [22]. Remarkably, the enriched

lipopolymer concentration is in excellent agreement with the value obtained from $\sigma_2 / \sigma^* = \sqrt{\varepsilon} \approx 2.7$. This high density $\sigma_2 > \sigma^*$ is also consistent with polycondensation of the lipopolymers which would potentially lead to lateral phase separation of lipopolymer and increase overlap significantly. Further, the local lipopolymer concentration and thickness within cushioned regions was independent of the total lipopolymer concentration of the system. The fraction of membrane supported by the hydrated polymer layer could be controlled; increasing ~0.12 per mol% of lipopolymer incorporated in the mixture. Extrapolating from this linear relationship, a homogenously cushioned membrane would be expected for mixtures containing 8.5 mol% of 2k MW PEG lipopolymer.

A further comment on the 65 Å thickness of the cushioned region is that it is only marginally larger than the uncushioned bilayer thickness. Thus, the bimodal distribution may also be partially stabilized from portions of the cushioned bilayer sitting atop the bilayer in contact with the underlying quartz substrate. Some support for this scenario comes from the structure of the membrane system at higher lipopolymer concentration. At 10 mol% a trimodal distribution was observed with the outermost membrane region located ~130 Å from the substrate (Fig. 4). This separation is only slightly less than a fully stretched PEG2k chain (158 Å) and would require an unphysically large lateral enrichment of lipopolymer. However, such a separation could result from continuation of the proposed bilayer stacking mechanism to a third layer. If the equilibrium cushion structure relies on overlapping membrane portions or

bilayer stacking, this may be a factor inhibiting the formation of complete homogenous cushions.

## *Conclusion:*

In this work NR and XR were used to structurally characterize supported lipid bilayers containing PEG lipopolymer. When the lipopolymer is functionalized with a reactive end-group, bimodally distributed cushion architectures were obtained. Without a strong binding interaction the lipopolymer is excluded from the inner leaflet of the membrane and a hydrated cushion was not obtained. While the reactive PEG system studied here did not yield homogenously cushioned membranes, these results demonstrate a method for creating full coverage membranes supported by laterally segregated, sub-micron cushions. Such platforms may prove useful for investigating the function of individual membrane proteins within isolated membrane microdomains. A thermodynamic description and accompanying phase diagram for lipopolymer membrane cushions show that these systems are highly tunable and can yield qualitatively different cushion architectures. For example, these systems can be manipulated into different regions within the phase diagram by changing surface charge density, altering the support material to modulate VDW interactions, or using reactive groups with different binding energies. Finally, other factors not captured by the thermodynamic description presented here may contribute to the equilibrium membrane cushion structure. For instance, cross-polymerization of the polymer tethering moieties may result in lateral phase separation of

cushioned membrane regions and bilayer stacking may also play a role in the final structure.

## *Acknowledgements:*

This work was supported by NSF Chemistry Division through grant CHE-0957868. Preliminary measurements were supported by NSF DMR-0606564. Neutron measurements were preformed at the SPEAR reflectometer at the Los Alamos Neutron Scattering Center (LANSCE). LANSCE is supported by DOE contract W7405-ENG-36 and the Advanced Photon Source by DOE contract W-31-109-Eng-38.We thank Doug Robinson for beam line assistance on beamline 6-ID at the Advanced Photon Source. We also thank Adrian Brozell for assistance with AFM measurements.

## *References:*

1. Castellana, E.T. and P.S. Cremer, *Solid supported lipid bilayers: From biophysical studies to sensor design*. Surface Science Reports, 2006. **61**(10): p. 429-444.
2. Sackmann, E. and M. Tanaka, *Supported membranes on soft polymer cushions: fabrication, characterization and applications*. Trends in Biotechnology, 2000. **18**(2): p. 58-64.
3. Tanaka, M. and E. Sackmann, *Polymer-supported membranes as models of the cell surface*. Nature, 2005. **437**(7059): p. 656-663.

4. Kiessling, V. and L.K. Tamm, *Measuring distances in supported bilayers by fluorescence interference-contrast microscopy: Polymer supports and SNARE proteins.* Biophysical Journal, 2003. **84**(1): p. 408-418.

5. Majewski, J., et al., *Structural studies of polymer-cushioned lipid bilayers.* Biophysical Journal, 1998. **75**(5): p. 2363-2367.

6. Naumann, C.A., et al., *Lateral mobility of phospholipids in tethered polymer-supported membranes.* Biophysical Journal, 2000. **78**(1): p. 273a-273a.

7. Naumann, C.A., et al., *The polymer-supported phospholipid bilayer: Tethering as a new approach to substrate-membrane stabilization.* Biomacromolecules, 2002. **3**(1): p. 27-35.

8. Wagner, M.L. and L.K. Tamm, *Tethered polymer-supported planar lipid bilayers for reconstitution of integral membrane proteins: Silane-polyethyleneglycol-lipid as a cushion and covalent linker.* Biophysical Journal, 2000. **79**(3): p. 1400-1414.

9. Smith, H.L., et al., *Model Lipid Membranes on a Tunable Polymer Cushion.* Physical Review Letters, 2009. **102**(22): p. -.

10. Albertorio, F., et al., *Fluid and air-stable lipopolymer membranes for biosensor applications.* Langmuir, 2005. **21**(16): p. 7476-7482.

11. Diaz, A.J., et al., *Double cushions preserve transmembrane protein mobility in supported bilayer systems.* Langmuir, 2008. **24**(13): p. 6820-6826.

12. Merzlyakov, M., et al., *Surface-supported bilayers with transmembrane proteins: Role of the polymer cushion revisited.* Langmuir, 2006. **22**(24): p. 10145-10151.

13. Rossi, C., et al., *Differential mechanisms for calcium-dependent protein/membrane association as evidenced from SPR-binding studies on supported biomimetic membranes.* Biochemistry, 2003. **42**(51): p. 15273-15283.

14. Kjaer, K., *Some Simple Ideas on X-Ray Reflection and Grazing-Incidence Diffraction from Thin Surfactant Films.* Physica B, 1994. **198**(1-3): p. 100-109.

15. Miller, C.E., J. Majewski, and T.L. Kuhl, *Characterization of single biological membranes at the solid-liquid interface by X-ray reflectivity.* Colloids and Surfaces a-Physicochemical and Engineering Aspects, 2006. **284**: p. 434-439.

16. Miller, C.E., et al., *Probing the local order of single phospholipid membranes using grazing incidence x-ray diffraction.* Physical Review Letters, 2008. **1**(5): p. -.

17. Watkins, E.B., et al., *Structure and Orientational Texture of Self-Organizing Lipid Bilayers.* Physical Review Letters, 2009. **102**(23): p. -.

18. Parratt, L.G., *Surface Studies of Solids by Total Reflection of X-Rays.* Physical Review, 1954. **95**(2): p. 359-369.

19. Pedersen, J.S. and I.W. Hamley, *Analysis of Neutron and X-Ray Reflectivity Data by Constrained Least-Squares Methods.* Physica B, 1994. **198**(1-3): p. 16-23.

20. Baekmark, T.R., et al., *Conformational Transitions of Mixed Monolayers of Phospholipids and Poly(Ethylene Oxide) Lipopolymers and Interaction Forces with Solid-Surfaces*. Langmuir, 1995. **11**(10): p. 3975-3987.

21. Kenworthy, A.K., et al., *Range and Magnitude of the Steric Pressure between Bilayers Containing Phospholipids with Covalently Attached Poly(Ethylene Glycol)*. Biophysical Journal, 1995. **68**(5): p. 1921-1936.

22. Kuhl, T.L., et al., *Modulation of Interaction Forces between Bilayers Exposing Short-Chained Ethylene-Oxide Headgroups*. Biophysical Journal, 1994. **66**(5): p. 1479-1488.

23. Kuhl, T.L., et al., *Packing stress relaxation in polymer-lipid monolayers at the air-water interface: An X-ray grazing-incidence diffraction and reflectivity study*. Journal of the American Chemical Society, 1999. **121**(33): p. 7682-7688.

24. Majewski, J., et al., *Structure of phospholipid monolayers containing poly(ethylene glycol) lipids at the air-water interface*. Journal of Physical Chemistry B, 1997. **101**(16): p. 3122-3129.

25. Charitat, T., et al., *Adsorbed and free lipid bilayers at the solid-liquid interface*. European Physical Journal B, 1999. **8**(4): p. 583-593.

26. Tanford, C., *Micelle Shape and Size*. Journal of Physical Chemistry, 1972. **76**(21): p. 3020-&.

27. Daniel, C., et al., *Structural characterization of an elevated lipid bilayer obtained by stepwise functionalization of a self-assembled alkenyl silane film*. Biointerphases, 2007. **2**(3): p. 109-118.

28. Israelachvili, J.N., *Intermolecular and Surface Forces*. 2nd ed ed. 1992, London: Academic Press.

29. Marra, J. and J. Israelachvili, *Direct Measurements of Forces between Phosphatidylcholine and Phosphatidylethanolamine Bilayers in Aqueous-Electrolyte Solutions*. Biochemistry, 1985. **24**(17): p. 4608-4618.

30. The distances used for the VDW calculations are the NR model separations between the substrate and hydrocarbon regions less 10A to account for the lipid head groups.

31. Grabbe, A. and R.G. Horn, *Double-Layer and Hydration Forces Measured between Silica Sheets Subjected to Various Surface Treatments*. Journal of Colloid and Interface Science, 1993. **157**(2): p. 375-383.

32. Developed by Grabbe, the algorithm explicitly computes the electrostatic potential between two flat surfaces using a relaxation method on a finite mesh.

33. Anderson, T.H., et al., *Formation of Supported Bilayers on Silica Substrates*. Langmuir, 2009. **25**(12): p. 6997-7005.

34. Kuhl, T.L., Leckband, D. E., Lasic, D. D., and Israelachvili, J. N., *Modulation of Interaction Forces Between Bilayers Exposing Short-Chained Ethylene Oxide Headgroups*. Biophysical Journal, 1994. **66**: p. 1479-1487

35. Moore, N.W. and T.L. Kuhl, *The role of flexible tethers in multiple ligand-receptor bond formation between curved surfaces*. Biophys J, 2006. **91**(5): p. 1675-87.

36. Sheth, S.R. and D. Leckband, *Measurements of attractive forces between proteins and end-grafted poly(ethylene glycol) chains*. Proc Natl Acad Sci U S A, 1997. **94**(16): p. 8399-404.

37. Wong, J.Y., et al., *Direct measurement of a tethered ligand-receptor interaction potential*. Science, 1997. **275**(5301): p. 820-2.

38. Wen, K., et al., *Postassembly chemical modification of a highly ordered organosilane multilayer: New insights into the structure, bonding, and dynamics of self-assembling silane monolayers*. Acs Nano, 2008. **2**(3): p. 579-599.